Preliminary Design Report

Trey Dufrene   Zack Johnson   David Orcutt   Alan Wallingford   Ryan Warner

Submitted in Partial Fulfillment of the Requirements of:

ME407 Preliminary Design – Fall 2019

Meiosis

College of Engineering
Embry-Riddle Aeronautical University
Prescott, AZ

Abstract

The Manipulator for Educational Institutions with Open Source Integrated Systems (MEIOSIS) aims to increase the accessibility of robotics to secondary educational institutions and hobbyists. Accordantly, the manipulator is 3D printed in PLA with aluminum tube supports and costs the end-user less than $1000. The manipulator has six links and a base. The base houses a Raspberry Pi 3B and power supply. The Raspberry Pi controls seven Dynamixel smart servos with position feedback and proportional derivative control. Six MX-12W servos actuate six rotational joints, while one AX-12A servo actuates the removable end-effector. They provide the manipulator a position repeatability within 2mm of the previous pose. The manipulator can draw as well as perform pick and place operations within its dexterous workspace which is a hemispherical sub-shell of the reachable workspace of 280 mm thickness. The manipulator's operation is controlled by open-source software.

Contents

1 Introduction 1
2 Requirements 1
3 Conceptual Design 3
4 Specifications 8
5 Preliminary Design 13
5.1 Computer Aided Design 13
5.2 Actuator Analysis 15
5.3 Forward Kinematics 17
5.4 Velocity Kinematics 19
5.5 Inverse Kinematics 19
5.6 Equations of Motion 20
5.7 Open-Loop Simulation 23
5.8 Closed-Loop Simulation 24
5.9 ANSYS 27
5.10 Electrical Schematic 30
5.11 Software Flowchart 30
5.12 Project Status and Future 34
5.13 Parts List 35

List of Figures

1 Overall System Conceptual Design . . . 3
2 Manipulator Base with Call-outs . . . 4
3 Drawing Showing Key Features of Design . . . 5
4 Drawing Showing Link Cross Section . . . 5
5 Electrical System Block Diagram . . . 6
6 Software Flowchart . . . 7
7 Overview of Physical System . . . 8
8 Elbow Manipulator Configuration with Link Offset . . . 9
9 Kinematic Model Representing Zeroed Configuration . . . 11
10 Manipulator in Zeroed Configuration with Callouts . . . 13
11 Link Cross Section . . . 14
12 Pulley 1-2 Center Distance . . . 15
13 Pulley 3 Center Distance . . . 15
14 Coordinate Systems . . . 17
15 Open-Loop Control Simulation Animation Snapshots . . . 23
16 Joint Angles vs Time in Open-Loop Simulation . . . 23
17 Joint Angles vs Time in Open-Loop Simulation . . . 24
18 Joint Angles vs Time in Open-Loop Simulation . . . 24
19 Closed-Loop Control Simulation Animation Snapshots . . . 26
20 Joint Angles vs Time in Closed-Loop Simulation . . . 26
21 Joint Angles vs Time in Closed-Loop Simulation . . . 26
22 Joint Angles vs Time in Closed-Loop Simulation . . . 27
23 T-Bar ANSYS FEA . . . 27
24 ANSYS Simulated Forces Image Capture . . . 28
25 ANSYS FEA of Dynamical Loading Scenario . . . 28
26 ANSYS Fatigue Test . . . 29
27 Electrical Schematic . . . 30
28 General Software Algorithm Overview . . . 31
29 Software Flowchart Subsections . . . 31
35 Cross Section of Dexterous Workspace Quadrant . . . 39

List of Tables

1 Manipulator Link 1 Mass Tabulations . . . 16
2 Manipulator Link 2 Mass Tabulations . . . 17
3 MEIOSIS Bill of Materials with Costs . . . 35
4 End-User Bill of Materials with Costs . . . 36

List Of Acronyms and Abbreviations

FK	:	Forward Kinematics
IK	:	Inverse Kinematics
PD	:	Proportional Derivative

Notation

${}^{\text{Frame}}_{\text{From}}r_{\text{To}}$	:	Direction Vectors
${}^{\text{From}}T_{\text{To}}$	:	Direction Cosine (Transformation) Matrices
$c_{\theta_{nm}}$	:	$\cos(\theta_n + \theta_m)$
$s_{\theta_{nm}}$	:	$\sin(\theta_n + \theta_m)$

1 Introduction

The Manipulator for Educational Institutions with Open Source Integrated Systems (MEIOSIS) aims to increase the accessibility of robotics education to high school students and hobbyists. Contained within this document is the design of a manipulator to fulfil this end. It will address the manipulator's conceptual design with requirements defining specification therefrom. A detailed design with motor descriptions introduces the manipulator's kinematics and simulations, concluding with a description of the system's operation and plans for implementation.

2 Requirements

The requirements of the system concisely define the capabilities the system must possess in order to solve the stated problem.

2.1 Hardware

The following requirements are hardware specific and dictate the physical constraints the system must adhere to.

2.1.1 The system shall cost the end-user no more than $1000.

2.1.2 The system shall be fully dexterous without being kinematically redundant.

To create a system with the intention of advancing education, it must be complex enough to encourage higher level problem solving, as well as be capable enough (dexterous) in a broad spectrum of tasks — in the interest of remaining useful in addition to retaining the interest of students.

2.1.3 The system end effector shall maintain a positional accuracy magnitude of ± 1 mm and an orientation accuracy of $\pm 5°$ eigen angle from the base frame.

To ensure that the robot has educational value, the accuracy must be defined so that any desired positions and movements are achieved.

2.1.4 The system end effector shall maintain a pose repeatability magnitude between 0.1—1.5 mm for the position and $\pm 4°$ eigen angle from the base frame for the orientation.

This is to ensure a robot that can execute the same movement commands repeatedly and have the same results every time.

2.1.5 The system's reachable workspace shall be a hemisphere with a radius of 300-700 mm.

This workspace will provide enough movement to manipulate objects in order to perform basic tasks.

2.1.6 The system's dexterous workspace shall contain a hemispherical shell within the reachable workspace with a thickness of 280 mm.

2.1.7 The system shall have a removable end effector capable of picking and placing a low-odor chisel tip Expo dry erase marker.

This creates a robot capable of performing a variety of basic tasks, which enhances its educational value.

2.1.8 The system shall be able to write with a low-odor chisel tip Expo dry erase marker.

2.2 Software

2.2.1 The system shall be open source.

This will create an easily obtainable, low cost method of distributing the system's source code, which may be modified for personal use.

2.2.2 The system shall be capable of operating given only desired end effector cartesian coordinates specified with respect to the base frame.

This simplicity makes the system of use to inexperienced users.

3 Conceptual Design

The terminator T-2000 is a science-fiction spectacle of a robot – until you see the price. Channeling the inspiration many high school students may have for robotics, MEIOSIS robotics aims to provide an affordable manipulator to educators and enthusiasts. MEIOSIS uses primarily 3-D printed components and easily accessible materials. Among these materials are a Raspberry PI, smart servos and metal tubing. These features create an open-source manipulator accessible to the public to further robotics education.

3.1 Physical System Overview

The physical design of the robotic manipulator will be shown through Figures *1, 2, 3,* and *4*.

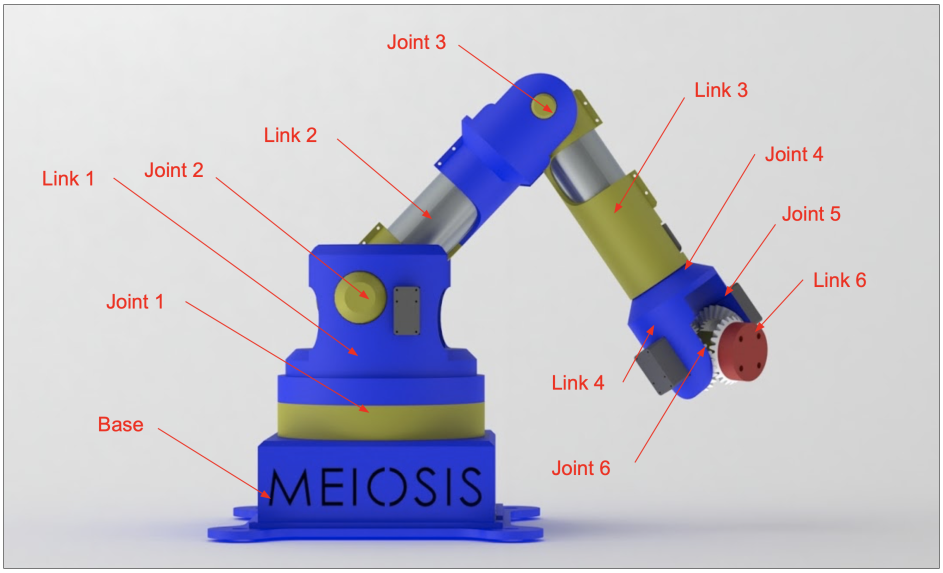

Figure 1: Overall System Conceptual Design

The colored links in *Figure 1* distinguish the different joints and links of the manipulator. The overall reach of the robot will be 582.5 mm. This length was chosen to decrease material cost and weight while still satisfying requirement 2.1.2 and 2.1.5, allowing the manipulating to pick and place objects to perform basic tasks. The base of the robot will be made to contain the Raspberry Pi and other electrical components.

3.1.1 Base

The base of the manipulator will house several of the electronic components, such as the computational system, power supply, and motor controller. A cross section of the base can be seen in *Figure 2*.

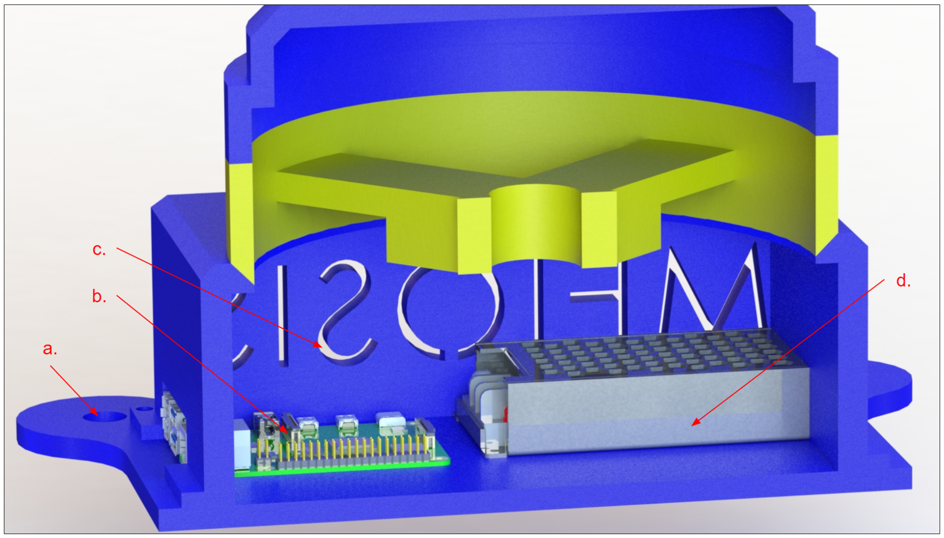

Figure 2: Manipulator Base with Call-outs

From *Figure 2*,

a. Base Supports: The base supports are located at each corner of the base and will allow the base of the manipulator to be securely attached to a variety of surfaces with either standard bolt/fastener hardware or suction cups.

b. Computational System: The computational system will be a Raspberry Pi; it will be housed in the base, which allows the Raspberry Pi to be more easily accessible. The primary reason for this system being chosen is to fulfill the budget requirement, 2.1.1. The Raspberry Pi will compute the manipulator's kinematics and command the motors accordingly.

c. Airflow Cutouts: The side of the base will have cutouts to allow for airflow through the base; since the power supply is housed inside of the base as well as the computational system, the temperature must be regulated to prevent overheating.

d. Power Supply: The power supply will be housed in the base as well; this allows the power supply to be more accessible and therefore more modifiable, so the end-user can easily expand the system to fulfill their needs.

3.1.2 Links

Figure 3 is an image of the robot that shows the links and their key features.

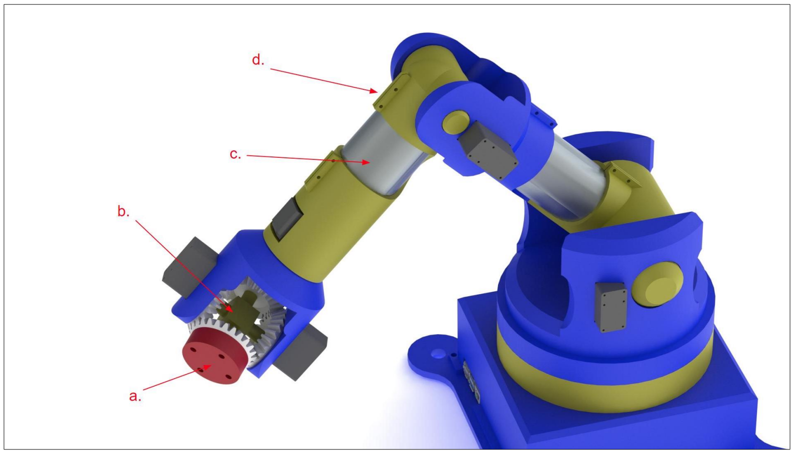

Figure 3: Drawing Showing Key Features of Design

Figure 3 highlights a few of the key features of our design. Call-out a shows the connection point for the end effector. The mountings are the standard used by the Sawyer manipulator. This may be adjusted to accommodate lower cost, more accessible end effectors. Call-out (b) shows the differential gearbox that will be used in the manipulator's wrist, saving space and weight. The manipulator will have aluminum tubing as support in the links (c) and will be attached to the 3D printed portion of the robot using clamp joints (d) tightened by screws.

Figure 4 is an image of the cross section of link 2 for the manipulator.

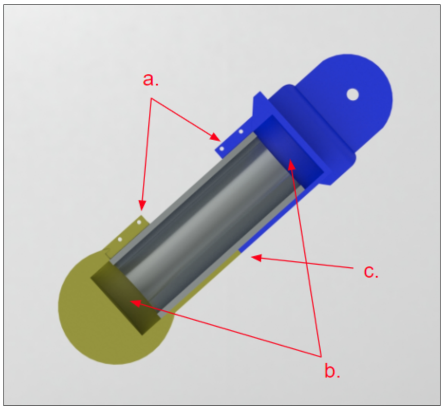

Figure 4: Drawing Showing Link Cross Section

The cross section seen in *Figure 4* shows the internal design for links two and three. It features two clamps that hold a hollow aluminum bar in place (a) and allows for gaps between the aluminum tube and the 3D printed call-out (b). The proper length will be dictated by the 3D printed guides lining up at call-out (c). This allows for imprecision in the manufacturing of the aluminum tube.

3.2 System Functions

The system can be divided into two subsystems: the electrical and software systems. The electrical subsystem includes the wiring and hardware computational components, power system, actuators with drivers, and sensors. The software subsystem includes the algorithm for the computational system.

3.3 Electrical

Figure 5 is the block diagram for the electrical system of the manipulator.

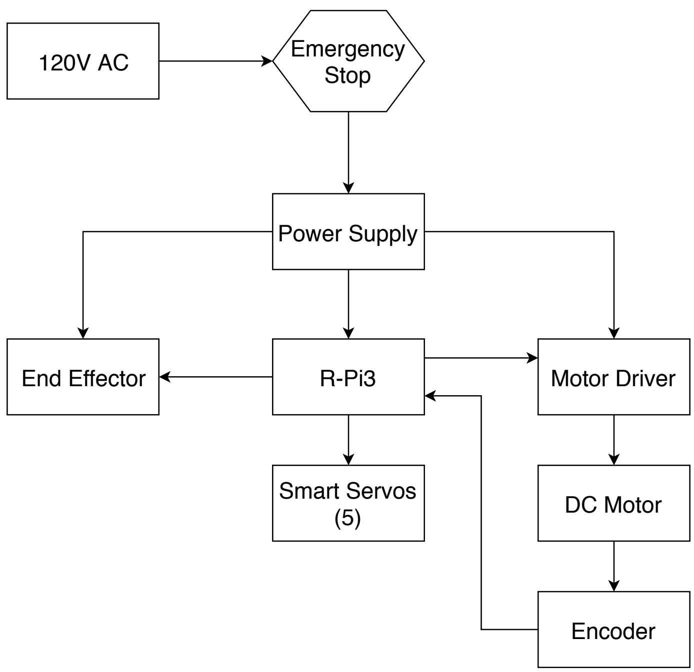

Figure 5: Electrical System Block Diagram

Figure 5 shows that the electrical systems of the manipulator will be relatively simple. Power is supplied by the 120V AC from standard wall outlets. A power supply will adapt the AC voltage to the required voltages for each component. One component is the Raspberry Pi, which will perform calculations for motor control (described below in software). It will send signals to the DC motor driver and the five smart servos. The smart servos have an on-board controller, so no feedback will be necessary. However, the first joint, between the base and the first link, will be actuated by a DC motor with an encoder to minimize cost.

3.4 Software

Figure 6 shows the software flowchart for the system.

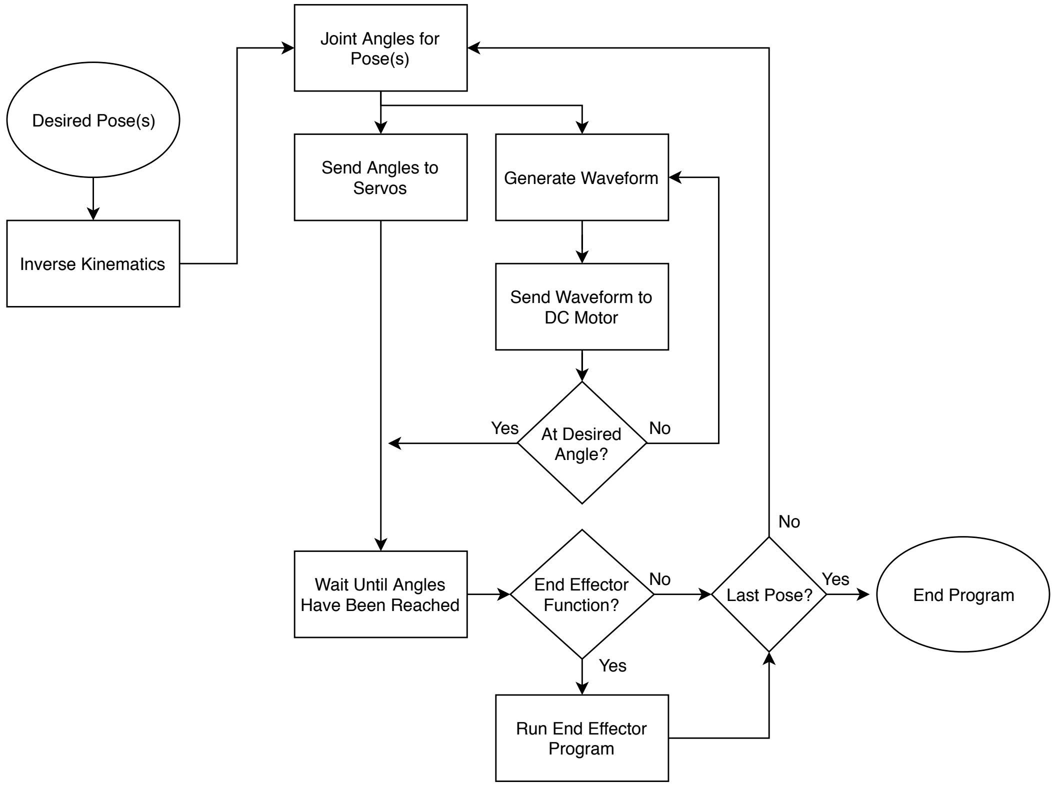

Figure 6: Software Flowchart

Similar to the electrical system, the software is also simple. *Figure 6* shows that the software will receive the desired pose or poses the user would like the manipulator to reach. Then the Raspberry Pi will use inverse kinematics to calculate the necessary joint angles. The waveforms/desired angles will be sent to the respective drivers/motors, and positional information will be sent back to the Raspberry Pi to adjust the DC motor angle. When the motors have reached their desired pose, the Raspberry Pi will actuate the end effector if it is specified by the user. The system will then check to see if there are any more poses to reach and either repeat the motor control section given the desired angles of the new pose or end program if the last pose has been reached.

4 Specifications

With the intention of making robotics education more accessible, The Manipulator for Educational Institutions with Open Source Integrated Systems (MEIOSIS) intends to provide high school educators and robot enthusiasts with a low cost manipulator. The system should be usable by novice students. It should also be modifiable to create a sustainably increased understanding of robotics. While MEIOSIS may not fully emulate industrial manipulators, it aims to provide more students with access to robotics education.

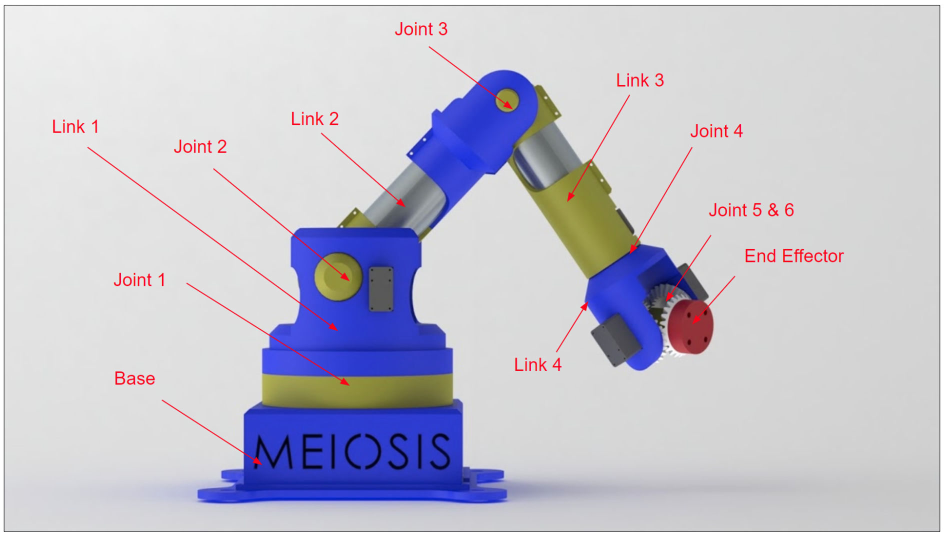

Figure 7: Overview of Physical System

The design seen in *Figure 7* is based on our conceptual design. It features four links and six joints for rotation and will be referenced throughout this document. The base of the manipulator and end-effector can also be seen in the figure.

4.1 Design Requirements

The specifications of the system are strictly based on the requirements defined previously. The requirements are divided into two primary categories, hardware and software.

4.2 Hardware

The following requirements and specifications are hardware specific and dictate the physical constaints the system must adhere to.

4.2.1 The system shall cost the end-user no more than $1000.

4.2.1.a The cost for the MEIOSIS team to develop the manipulator shall cost no more than $800.

4.2.2 The system shall be fully dexterous without being kinematically redundant.

4.2.2.a The system shall consist of six rotational joints connected by four links. The last three joints will create a spherical wrist.

As defined [2], "A manipulator having more than six DOF is referred to as a kinematically redundant manipulator (5)." A manipulator with less than six degrees of freedom will not be fully dexterous within it's workspace. *Figure 9* (see subsection 4.2.6, p. 11) shows a six degree-of-freedom rotary manipulator with it's coordinate frames in zeroed positions. The joint and link locations are seen in *Figure 7* (see section 4, p. 8).

4.2.2.b The system shall have no link offsets.

Link offsets as seen in *Figure 8* are commonly used to avoid singularities. However, having a link offset prevents the manipulator's dexterous workspace from being a complete hemispherical shell.

Figure 8: Elbow Manipulator Configuration with Link Offset [2]

As shown in *Figure 8*, the line directly above the first joint of the manipulator is offset such that the axes of the other joints are unable to become collinear with the base axis; this prevents singularity but causes a void in the detxterous workspace.

4.2.3 The system end effector shall maintain a positional accuracy magnitude of ± 1 mm and an orientation accuracy of $\pm 5°$ eigen angle from the base frame.

To ensure that the robot has educational value, the accuracy must be defined so that any desired positions and movements are achieved.

4.2.3.a The system shall accommodate a process in which the end user can calibrate the *end effector position and orientation to within 0.5 mm and 1 degree of the manipulator's precision.*

The addition of a calibration process allows the removal of any systematic errors, such as drift. The theoretical limit of the calibration process is the difference between the precision and accuracy metrics of the system.

4.2.4 The system end effector shall maintain a pose repeatability magnitude between 0.1—1.5 mm for the position and $\pm 4°$ eigen angle from the base frame for the orientation.

4.2.4.a Joint one and two of the system shall possess an angle error of no more than .025 degrees.

Being that joint one and two are the first two rotational elements in the system, their error will propagate the most to the end effector's position.

4.2.4.b Joint three of the system shall possess an angle error of no more than .03 degrees.

Since joint three is closer to the end effector it's error will not propagate as severely throughout the system.

4.2.4.c Joints four, five, and six shall possess an angle error of no more than .29 degrees.

The spherical wrist is the closest to the end effector's final position and therefore has the least error propagation.

4.2.5 The system's reachable workspace shall be a hemisphere with a radius of 300-700 mm.

This workspace will provide enough movement to manipulate objects in order to perform basic tasks.

4.2.5.a The length of link one, two, three, four, and the wrist shall be 220.8 mm, 250 mm, 200 mm, 80 mm, and 52.5 mm respectively.

This results in a total height of 220.8 mm with a total reach of 582.5 mm in the zeroed configuration as shown in the configuration represented in *Figure 9*.

4.2.6 The system's dexterous workspace shall contain a hemispherical shell within the reachable workspace with a thickness of 280 mm.

This workspace will provide enough movement to manipulate objects in order to perform basic tasks. 280mm is slightly greater than the length of letter paper.

4.2.6.a The rotational limit of joint one, two, three, four, five, and six shall be $\pm 180°$, $-9.7°$

to 177.5°*,* −150.6° *to* −19.3°*,* ±180°*,* −180° *to* −1.6°*, and* ±180° *respectively.*

The angles stated are with respect to the kinematic model shown in *Figure 9*. To be fully dexterous within our 280 mm dexterous workspace the manipulator must have the joint angles specified above. The joint limitations were calculated by iteratively verifying the orientation about every point within the quarter hemisphere cross section seen in *Figure 35* (see Appendix, p. 39).

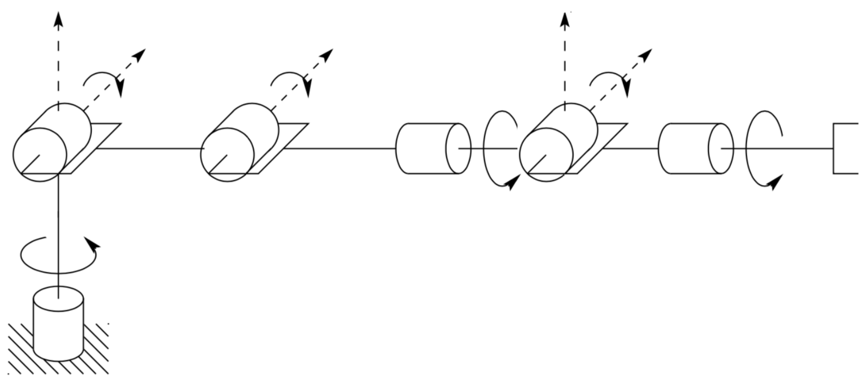

Figure 9: Kinematic Model Representing Zeroed Configuration [2]

4.2.7 The system shall have a removable end effector capable of picking and placing a low-odor chisel tip Expo dry erase marker.

This creates a robot capable of performing a variety of basic tasks, which enhances its educational value.

4.2.7.a The system shall use a parallel gripper that can close to 18mm.

The diameter of a low-odor chisel tip Expo dry erase marker is approximately 18 mm.

4.2.7.b The end effector shall attach to the manipulator using screws configured in a pattern that can accommodate a Dynamixel AX-12A servo.

It is expected that a majority of end effector styles will have to accommodate for a servo to facilitate actuation, therefore a pattern was chosen to standardize the mounting.

4.2.8 The system shall be able to write with a low-odor chisel tip Expo dry erase marker.

4.2.8.a The end effector shall be able to support 0.004 Newton meter moments about the axes normal to its gripping surfaces.

The coefficient of friction between the Expo marker and paper can be approximated and given the weight of an Expo marker the approximate grip strength of the end effector can be calculated.

4.3 Software

The following requirements and specifications are software specific and determine the attributes of the operating system.

4.3.1 The system shall be open source.

This will create an easily obtainable, low cost method of distributing the system's source code, which may be modified for personal use.

4.3.1.a The software shall be hosted publicly on an online repository and maintain an MIT license for distribution.

This allows the end-user to freely download and modify the code without licensing. The MIT license disregards any legal obligation to code upkeep and documentation by the original author.

4.3.2 The system shall be capable of operating given only desired end effector cartesian coordinates specified with respect to the base frame.

4.3.2.a The system shall have a user interface capable of accepting the end-effector's desired cartesian position and Euler angle orientation as a six element row vector.

The system software interface facilitates an untrained user to operate without the advanced knoledge of the system's kinematics.

4.3.2.b The system shall be capable of performing floating point arithmetic.

The solution for the inverse kinematics requires the ability to perform high level arithmetic with little error.

5 Preliminary Design

The preliminary design section represents the most up-to-date status of the project and also encompasses information pertaining to several different specific design choices that had to be considered. The computer aided design section contains information regarding the physical design of the manipulator as well as noting key design features; the actuator analysis section contains information regarding actuator considerations and calculations being that the servo motors play an essential role in the functionality of the final system.

5.1 Computer Aided Design

The manipulator will be six degrees of freedom and will feature a spherical wrist. This design incorporates two different differential drive gearboxes that each control two degrees of freedom. This is to reduce the amount of required torques from the motors on the shoulder joint and reduce size in the wrist. In order to achieve accuracy requirements, timing belts are incorporated into the design in order to control the first three degrees of freedom. The following figure shows the join configuration used in the design of the manipulator.

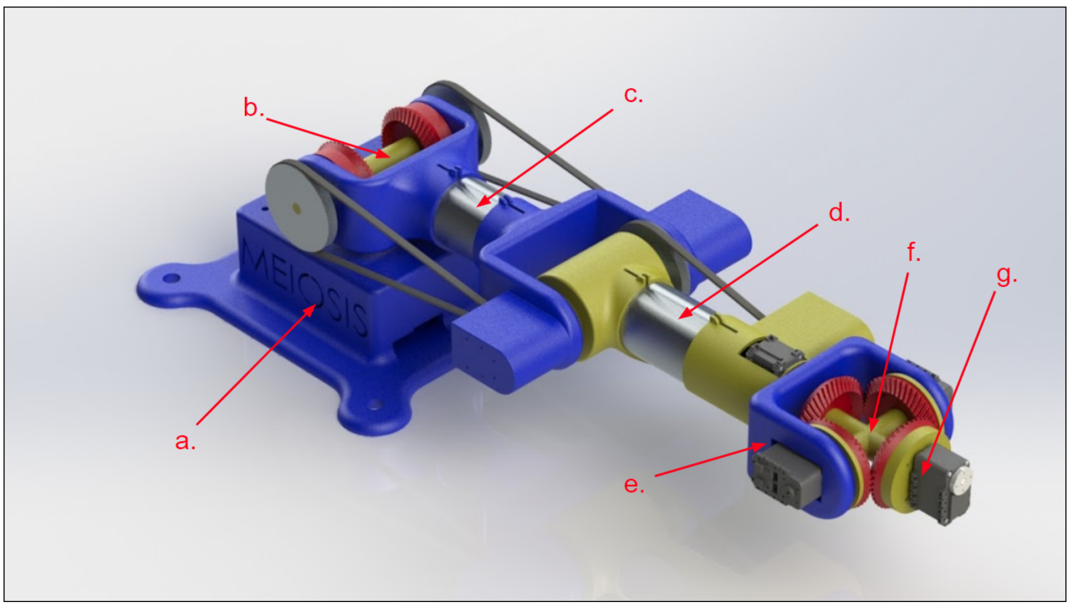

Figure 10: Manipulator in Zeroed Configuration with Callouts

Figure 10 shows the zeroed configuration for the manipulator with callouts showing the link locations.

a. The *Manipulator Base* is designed to hold the Raspberry Pi and power supply. The base features holes for airflow and I/O connections.

b. Link 1 & Differential Drive have three bevel gears to create the first differential drive rotational joint of the manipulator.

c. Link 2 has servos located at the end of the link to control the movement for the first two degrees of freedom at the shoulder and are connected to link 1 using timing belts.

d. Link 3 contains two servos attached to the link that control the third degree of freedom (the elbow) and the fourth degree of freedom which is the first degree of freedom for the wrist.

e. Link 4 houses the servos used to control the fifth and sixth degree of freedom, which are both in the wrist's differential drive gearbox.

f. Link 5 provides support for the wrist's differential drive gearbox.

g. The *End Effector* features connection points to hold a Dynamixel AX-12A smart servo.

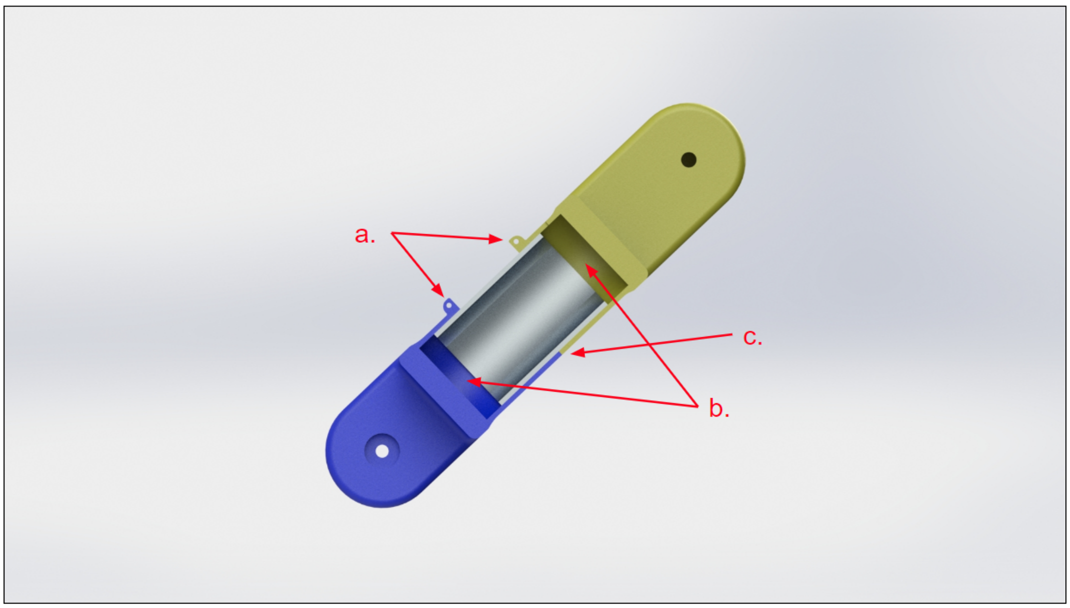

Figure 11: Link Cross Section

Figure 11 shows the cross-section for link two with callouts for key features in the design.

a. Clamping mechanisms connect the aluminum pipe to the 3-D printed parts. This will allow for an easy way to assemble the manipulator while allowing for a large amount of tolerance in the length of the pipe when manufacturing the part.

b. Shows an example of the gaps between the aluminum pipe and the 3-D printed parts.

c. Shows where the 3-D printed parts will line up to ensure that the link is the correct length and orientation.

5.1.1 Pulleys

A 12 tooth and 120 tooth pulleys provide a 10:1 gear ratio and use a 0.25 in wide MXL belt. The center distance between the pulleys must be at least 5.43 in to have 5 teeth meshing. Because of the high gear ratio, greater distances do not increase the number of teeth in mesh. *Figure 12* shows the distance between the manipulator's first two pulleys is 235.185 mm or 9.259 in, which corresponds to a belt with 300 and pitch diameter of 24 in. *Figure*

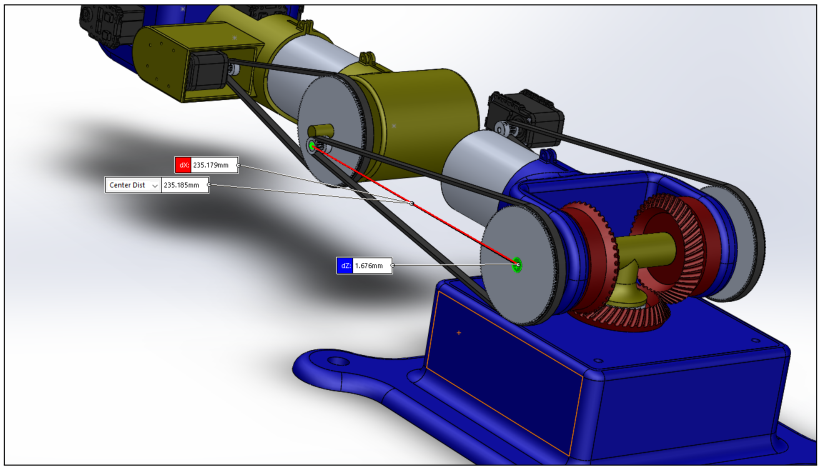

Figure 12: Pulley 1-2 Center Distance

13 shows the center distance between the second pulleys is 139.960 mm or 5.510 in. The corresponding belt has 208 teeth with a 16.6 in pitch diameter.

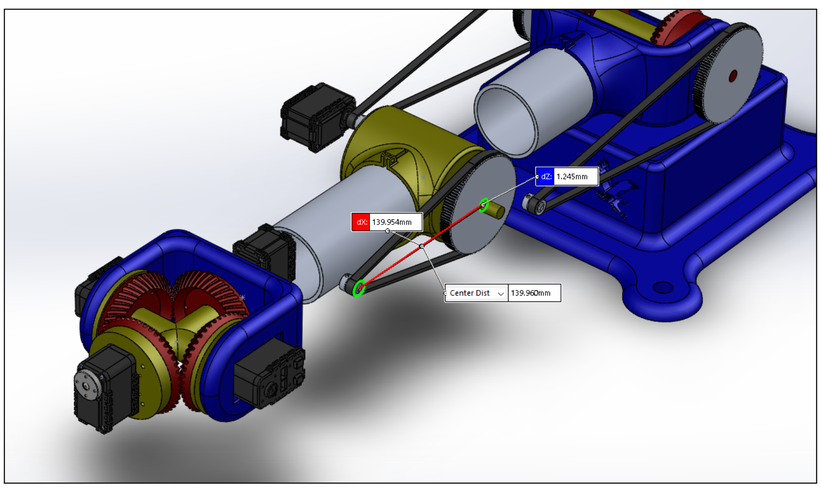

Figure 13: Pulley 3 Center Distance

5.2 Actuator Analysis

Dynamixel does not provide a stall torque for the MX-12W servo, however it does provide stall torque data for two similar servos. The MX-12W's stall torque can be found from the stall torque data since the motor are the same. The stall torque of the MX-12W should be comparable to the AX-12W's stall torque. The MX-12W and AX-12W operate at the same 12 V voltage, 32:1 gear ratio, and 470 rpm no load output speed. The AX-12A also operates at 12 V, but at with a 254:1 gear ratio and 59 rpm no load output speed. Torque and current are inversely related. If the AX-12A's and AX-12W's motors are the same, then when operating at the same voltage, the output speed of the AX-12W should equal to the output speed of the AX-12A multiplied by the ratio of the servos' gear ratios and the torque of the AX-12W should be the AX-12A's torque multiplied by the inverse of the gear ratios ratio:

$$59 \cdot \frac{254}{32} = 468 \cong 470$$

The AX-12A's and MX-12W's stall torques are 1.5Nm and 0.21Nm, respectively [3]:

$$1.5 \cdot \frac{32}{254} = 0.189 \cong 0.21\text{Nm}$$

Therefore, the AX-12A and MX-12W use the same motor. Additionally, if operating at the same voltage, the stall torque is defined by the no load output speed and gear ratio. Since the MX-12W and AX-12A operate at the same 12 V voltage with the same 32:1 gear ratio and 470 rpm no load output speed, their stall torques should be the same. More specifically, it is between the AX-12W's and the gear reduced AX-12A's stall torques of 0.21Nm and 0.189Nm, respectively. Therefore, the stall MX-12W's stall torque is within 0.01Nm of 0.2Nm. The manipulator is designed for the worst case scenario: 0.19 Nm.

The first differential has its greatest torque when the manipulator is in the zeroed configuration. In the zeroed configuration, the arm is outstretched with gravity acting perpendicular to the arm's length. Since the manipulator must only support a chisel tip dry erase Expo marker, the maximum torque may be approximated as the manipulator's arm's mass acting acting near the centroid. More mass from the servos and longer aluminum support in link 3 place the center of mass closer to the end-effector than the base. Therefore, the point at which the arm's mass acts is assumed to be 273 mm from the base. These calculations will be further revised with mass parameters from the STL files generating the open and closed loop simulations. *Table 1* estimates the manipulator's arm's mass.

Table 1: Manipulator Link 1 Mass Tabulations

Item	**Specifications**	**Weight (g)**	**Notes**
3-D Printed Materials	30% infill	353	100% infill: 1177g
Servos	7 low torque	385	55 $^{g}/_{servo}$
Aluminum Support	.75″ OD .125″ thick 1′ long	287	44.23 $^{g}/_{in^3}$
Bearings	5 bearings	60	12 $^{g}/_{bearing}$
End Effector		50	Approx.
Safety Factor		205	
	Total	1340	

The total mass of 1340g as seen in *Table 1* yields a moment of 0.361 Nm or 3.685 kgm. To generate smooth motions, Dynamixel recommends operating at one fifth of the stall torque. Therefore, the actual maximum required torque is 1.805 Nm. An MX-12W provides 0.19 Nm of torque, necessitating a 10:1 gear ratio. While the AX-12A provides a greater torque of 1.5 Nm, it would also require gearing. It is only precise to 0.8 degrees, while the specifications require at least 0.29 degrees of precision for joints one and two. Further, the AX-12A only receives position feedback for 300 degrees of its rotation and cannot track multiple rotations, making it untenable for the base motor, which must rotate more than 360 degrees.

The third joint's torque requirements can be approximated in the same manner. However, links three, four, and five's masses are assumed to act 200 mm from the third joint 3. *Table 2* estimates the links' masses.

Table 2: Manipulator Link 2 Mass Tabulations

Item	**Specifications**	**Weight (g)**	**Notes**
3-D Printed Materials	30% infill	180	100% infill: 1177g
Servos	4 low torque	220	55 g/servo
Aluminum Support	.75″ OD .125″ thick 1′ long	140	44.23 $^{g}/_{in^3}$
Bearings	5 bearings	36	12 g/bearing
End Effector		50	Approx.
Safety		205	
	Total	831	

The resulting moment is 1.630 Nm, which can be satisfied by the same motor and gear ratio used on the base.

5.3 Forward Kinematics

The forward kinematics of the manipulator are described by the equations below, where the reference coordinate frames are given by *Figure 14*.

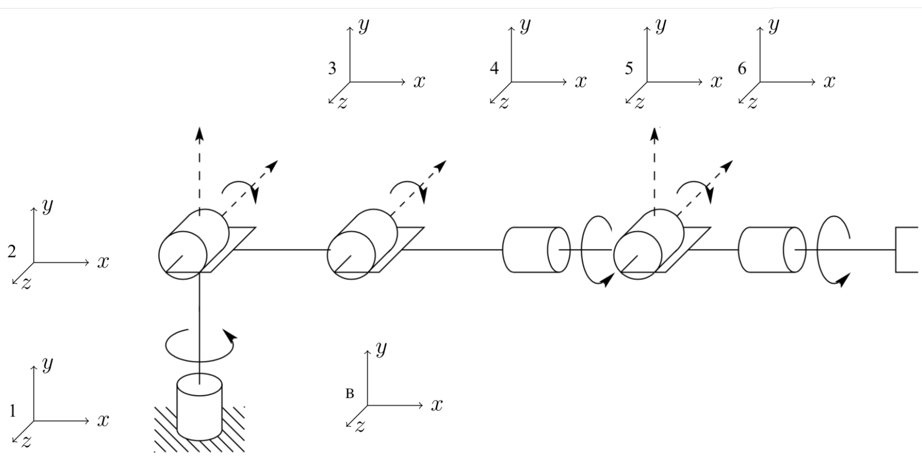

Figure 14: Coordinate Systems

Given the direction cosine matrices,

$$rotx(\theta) = \begin{bmatrix} 1 & 0 & 0 \\ 0 & \cos(\theta) & -\sin(\theta) \\ 0 & \sin(\theta) & \cos(\theta) \end{bmatrix} \quad , \quad roty(\theta) = \begin{bmatrix} 1 & 0 & 0 \\ 0 & \cos(\theta) & -\sin(\theta) \\ 0 & \sin(\theta) & \cos(\theta) \end{bmatrix}$$

$$rotz(\theta) = \begin{bmatrix} \cos(\theta) & 0 & \sin(\theta) \\ 0 & 1 & 0 \\ -\sin(\theta) & \cos(\theta) & 0 \end{bmatrix}$$

The orientation of each link with respect to the inertial frame is given as:

$$\begin{aligned}
{}^{I}T_1 &= rotz(\theta_1) \\
{}^{I}T_2 &= rotz(\theta_1)\ rotx(\theta_2) \\
{}^{I}T_3 &= rotz(\theta_1)\ rotx(\theta_2)\ rotx(\theta_3) \\
{}^{I}T_4 &= rotz(\theta_1)\ rotx(\theta_2)\ rotx(\theta_3)\ roty(\theta_4) \\
{}^{I}T_5 &= rotz(\theta_1)\ rotx(\theta_2)\ rotx(\theta_3)\ roty(\theta_4)\ rotx(\theta_5) \\
{}^{I}T_6 &= rotz(\theta_1)\ rotx(\theta_2)\ rotx(\theta_3)\ roty(\theta_4)\ rotx(\theta_5)\ roty(\theta_6)
\end{aligned}$$

$${}^{I}T_1 = \begin{bmatrix} c_{\theta_1} & -s_{\theta_1} & 0 \\ s_{\theta_1} & c_{\theta_1} & 0 \\ 0 & 0 & 1 \end{bmatrix} \quad {}^{I}T_2 = \begin{bmatrix} c_{\theta_1} & -c_{\theta_2} s_{\theta_1} & s_{\theta_1} s_{\theta_2} \\ s_{\theta_1} & c_{\theta_1} c_{\theta_2} & -c_{\theta_1} s_{\theta_2} \\ 0 & s_{\theta_2} & c_{\theta_2} \end{bmatrix} \quad {}^{I}T_3 = \begin{bmatrix} c_{\theta_1} & -c_{\theta_{23}} s_{\theta_1} & s_{\theta_{23}} s_{\theta_1} \\ s_{\theta_1} & c_{\theta_{23}} c_{\theta_1} & -s_{\theta_{23}} c_{\theta_1} \\ 0 & s_{\theta_{23}} & c_{\theta_{23}} \end{bmatrix}$$

$${}^{I}T_4 = \begin{bmatrix} c_{\theta_1} c_{\theta_4} - s_{\theta_{23}} s_{\theta_1} s_{\theta_4} & -c_{\theta_{23}} s_{\theta_1} & c_{\theta_1} s_{\theta_4} + s_{\theta_{23}} c_{\theta_4} s_{\theta_1} \\ c_{\theta_4} s_{\theta_1} + s_{\theta_{23}} c_{\theta_1} s_{\theta_4} & c_{\theta_{23}} c_{\theta_1} & s_{\theta_1} s_{\theta_4} - s_{\theta_{23}} c_{\theta_1} c_{\theta_4} \\ -c_{\theta_{23}} s_{\theta_4} & s_{\theta_{23}} & c_{\theta_{23}} c_{\theta_4} \end{bmatrix}$$

$${}^{I}T_5 = \begin{bmatrix} c_{\theta_1} c_{\theta_4} - s_{\theta_{23}} s_{\theta_1} s_{\theta_4} & s_{\theta_5}(c_{\theta_1} s_{\theta_4} + s_{\theta_{23}} c_{\theta_4} s_{\theta_1}) - c_{\theta_{23}} c_{\theta_5} s_{\theta_1} & c_{\theta_5}(c_{\theta_1} s_{\theta_4} + s_{\theta_{23}} c_{\theta_4} s_{\theta_1}) + c_{\theta_{23}} s_{\theta_1} s_{\theta_5} \\ c_{\theta_4} s_{\theta_1} + s_{\theta_{23}} c_{\theta_1} s_{\theta_4} & s_{\theta_5}(s_{\theta_1} s_{\theta_4} - s_{\theta_{23}} c_{\theta_1} c_{\theta_4}) + c_{\theta_{23}} c_{\theta_1} c_{\theta_5} & c_{\theta_5}(s_{\theta_1} s_{\theta_4} - s_{\theta_{23}} c_{\theta_1} c_{\theta_4}) - c_{\theta_{23}} c_{\theta_1} s_{\theta_5} \\ -c_{\theta_{23}} s_{\theta_4} & s_{\theta_{23}} c_{\theta_5} + c_{\theta_{23}} c_{\theta_4} s_{\theta_5} & c_{\theta_{23}} c_{\theta_4} c_{\theta_5} - s_{\theta_{23}} s_{\theta_5} \end{bmatrix}$$

$${}^{I}T_6 = \begin{bmatrix} {}^{I}T_{6(1,1)} & {}^{I}T_{6(1,2)} & {}^{I}T_{6(1,3)} \\ {}^{I}T_{6(2,1)} & {}^{I}T_{6(2,2)} & {}^{I}T_{6(2,3)} \\ {}^{I}T_{6(3,1)} & {}^{I}T_{6(3,2)} & {}^{I}T_{6(3,3)} \end{bmatrix}$$

$$\begin{aligned}
{}^{I}T_{6(1,1)} &= c_{\theta_6}(c_{\theta_1} c_{\theta_4} - s_{\theta_{23}} s_{\theta_1} s_{\theta_4}) - s_{\theta_6}(c_{\theta_5}(c_{\theta_1} s_{\theta_4} + s_{\theta_{23}} c_{\theta_4} s_{\theta_1}) + c_{\theta_{23}} s_{\theta_1} s_{\theta_5}) \\
{}^{I}T_{6(1,2)} &= s_{\theta_5}(c_{\theta_1} s_{\theta_4} + s_{\theta_{23}} c_{\theta_4} s_{\theta_1}) - c_{\theta_{23}} c_{\theta_5} s_{\theta_1} \\
{}^{I}T_{6(1,3)} &= c_{\theta_6}(c_{\theta_5}(c_{\theta_1} s_{\theta_4} + s_{\theta_{23}} c_{\theta_4} s_{\theta_1}) + c_{\theta_{23}} s_{\theta_1} s_{\theta_5}) + s_{\theta_6}(c_{\theta_1} c_{\theta_4} - s_{\theta_{23}} s_{\theta_1} s_{\theta_4}) \\
{}^{I}T_{6(2,1)} &= c_{\theta_6}(c_{\theta_4} s_{\theta_1} + s_{\theta_{23}} c_{\theta_1} s_{\theta_4}) - s_{\theta_6}(c_{\theta_5}(s_{\theta_1} s_{\theta_4} - s_{\theta_{23}} c_{\theta_1} c_{\theta_4}) - c_{\theta_{23}} c_{\theta_1} s_{\theta_5}) \\
{}^{I}T_{6(2,2)} &= s_{\theta_5}(s_{\theta_1} s_{\theta_4} - s_{\theta_{23}} c_{\theta_1} c_{\theta_4}) + c_{\theta_{23}} c_{\theta_1} c_{\theta_5} \\
{}^{I}T_{6(2,3)} &= s_{\theta_6}(c_{\theta_4} s_{\theta_1} + s_{\theta_{23}} c_{\theta_1} s_{\theta_4}) + c_{\theta_6}(c_{\theta_5}(s_{\theta_1} s_{\theta_4} - s_{\theta_{23}} c_{\theta_1} c_{\theta_4}) - c_{\theta_{23}} c_{\theta_1} s_{\theta_5}) \\
{}^{I}T_{6(3,1)} &= s_{\theta_6}(s_{\theta_{23}} s_{\theta_5} - c_{\theta_{23}} c_{\theta_4} c_{\theta_5}) - c_{\theta_{23}} c_{\theta_6} s_{\theta_4} \\
{}^{I}T_{6(3,2)} &= s_{\theta_{23}} c_{\theta_5} + c_{\theta_{23}} c_{\theta_4} s_{\theta_5} \\
{}^{I}T_{6(3,3)} &= c_{\theta_6}(s_{\theta_{23}} s_{\theta_5} - c_{\theta_{23}} c_{\theta_4} c_{\theta_5}) - c_{\theta_{23}} s_{\theta_4} s_{\theta_6}
\end{aligned}$$

Given the lengths of each of the manipulator links,

$$ {}^{I}_{B}r_1 = \begin{bmatrix} 0 \\ 0 \\ \ell_b \end{bmatrix} \quad {}^{1}_{1}r_2 = \begin{bmatrix} 0 \\ 0 \\ \ell_1 \end{bmatrix} \qquad {}^{2}_{2}r_3 = \begin{bmatrix} 0 \\ \ell_2 \\ 0 \end{bmatrix} \quad {}^{3}_{3}r_4 = \begin{bmatrix} 0 \\ \ell_3 \\ 0 \end{bmatrix} \qquad {}^{4}_{4}r_5 = \begin{bmatrix} 0 \\ \ell_4 \\ 0 \end{bmatrix} \quad {}^{5}_{5}r_6 = \begin{bmatrix} 0 \\ \ell_5 \\ 0 \end{bmatrix} $$

The position of each link relative to the inertial frame is given as:

$$ \begin{array}{lll} {}^{I}_{B}r_1 = {}_{B}r_1 & {}^{I}_{B}r_2 = r_1 + {}^{I}T_1{}^{1}_{1}r_2 & {}^{I}_{B}r_3 = r_2 + {}^{I}T_2{}^{2}_{2}r_3 \\ {}^{I}_{B}r_4 = r_3 + {}^{I}T_3{}^{3}_{3}r_4 & {}^{I}_{B}r_5 = r_4 + {}^{I}T_4{}^{4}_{4}r_5 & {}^{I}_{B}r_6 = r_5 + {}^{I}T_5{}^{5}_{5}r_6 \end{array} $$

$$ {}^{I}_{B}r_1 = \begin{bmatrix} 0 \\ 0 \\ \ell_b \end{bmatrix} \qquad {}^{I}_{B}r_2 = \begin{bmatrix} 0 \\ 0 \\ \ell_b + \ell_1 \end{bmatrix} \quad {}^{I}_{B}r_3 = \begin{bmatrix} -\ell_2 c_{\theta_2} s_{\theta_1} \\ \ell_2 c_{\theta_{12}} \\ \ell_b + \ell_1 + \ell_2 s_{\theta_2} \end{bmatrix} \qquad {}^{I}_{B}r_4 = \begin{bmatrix} -s_{\theta_1}(\ell_3 c_{\theta_{23}} + \ell_2 c_{\theta_2}) \\ c_{\theta_1}(\ell_3 c_{\theta_{23}} + \ell_2 c_{\theta_2}) \\ \ell_1 + \ell_b + \ell_3 s_{\theta_{23}} + \ell_2 s_{\theta_2} \end{bmatrix} $$

$$ {}^{I}_{B}r_5 = \begin{bmatrix} -s_{\theta_1}(\ell_3 c_{\theta_{23}} + \ell_4 c_{\theta_{23}} + \ell_2 c_{\theta_2}) \\ c_{\theta_1}(\ell_3 c_{\theta_{23}} + \ell_4 c_{\theta_{23}} + \ell_2 c_{\theta_2}) \\ \ell_1 + \ell_b + \ell_3 s_{\theta_{23}} + \ell_4 s_{\theta_{23}} + \ell_2 s_{\theta_2} \end{bmatrix} $$

$$ {}^{I}_{B}r_6 = \begin{bmatrix} \ell_5 c_{\theta_1} s_{\theta_4} s_{\theta_5} - \ell_4 c_{\theta_{23}} s_{\theta_1} - \ell_2 c_{\theta_2} s_{\theta_1} - \ell_5 c_{\theta_{23}} c_{\theta_5} s_{\theta_1} - \ell_3 c_{\theta_{23}} s_{\theta_1} \\ \quad + \ell_5 c_{\theta_2} c_{\theta_4} s_{\theta_1} s_{\theta_3} s_{\theta_5} + \ell_5 c_{\theta_3} c_{\theta_4} s_{\theta_1} s_{\theta_2} s_{\theta_5} \\ \ell_5(s_{\theta_5}(s_{\theta_1} s_{\theta_4} - c_{\theta_4}(c_{\theta_1} c_{\theta_2} s_{\theta_3} + c_{\theta_1} c_{\theta_3} s_{\theta_2})) - c_{\theta_5}(c_{\theta_1} s_{\theta_2} s_{\theta_3} - c_{\theta_1} c_{\theta_2} c_{\theta_3})) \\ \quad - \ell_3(c_{\theta_1} s_{\theta_2} s_{\theta_3} - c_{\theta_1} c_{\theta_2} c_{\theta_3}) - \ell_4(c_{\theta_1} s_{\theta_2} s_{\theta_3} - c_{\theta_1} c_{\theta_2} c_{\theta_3}) + \ell_2 c_{\theta_1} c_{\theta_2} \\ \ell_1 + \ell_b + \ell_3 s_{\theta_{23}} + \ell_4 s_{\theta_{23}} + \ell_2 s_{\theta_2} + \dfrac{\ell_5 c_{\theta_{23}} s_{\theta_{45}}}{2} + \ell_5 s_{\theta_{23}} c_{\theta_5} - \dfrac{\ell_5 s_{\theta_4 - \theta_5} c_{\theta_{23}}}{2} \end{bmatrix} $$

5.4 Velocity Kinematics

The translational and rotational velocties ($\dot{r}$ & ω) can be found given the geometric jacobian of the body and transformation matrix corresponding to it.

$$ \begin{bmatrix} {}^{B}_{B}\omega_I \\ {}^{I}_{B}\dot{r}_B \end{bmatrix} = J_B = \begin{bmatrix} {}^{I}T_B(:,3)^T \cdot \dfrac{\partial}{\partial\gamma}{}^{I}T_B(:,2) \\ {}^{I}T_B(:,1)^T \cdot \dfrac{\partial}{\partial\gamma}{}^{I}T_B(:,3) \\ {}^{I}T_B(:,2)^T \cdot \dfrac{\partial}{\partial\gamma}{}^{I}T_B(:,1) \end{bmatrix} $$

5.5 Inverse Kinematics

The inverse kinematics can be calculated given desired position and orientation vectors, o and R, respecitvely.

$$ \begin{bmatrix} x_c & y_c & z_c \end{bmatrix} = o \;, \quad R = \begin{bmatrix} r_{11} & r_{12} & r_{13} \\ r_{21} & r_{22} & r_{23} \\ r_{31} & r_{32} & r_{33} \end{bmatrix} $$

Inverse Position:

$$\theta_1 = \text{atan2}\left(x_c,\ y_c\right) - {}^{\pi}/_{2}$$
$$\theta_2 = \text{atan2}\left(z_c - \ell_1,\ \sqrt{x_c^2 + y_c^2}\right) - \text{atan2}\left(\ell_3 s_3,\ \ell_2 + \ell_3 c_3\right)$$
$$\theta_3 = \text{atan2}(-\sqrt{1 - D^2},\ D)$$
$$\text{where } D \equiv \frac{x_c^2 + y_c^2 + (z_c - \ell_1)^2 - \ell_2^2 - \ell_3^2}{2\ell_2\ell_3}$$

Inverse Orientation :

$$^{I}T_3 = rotz(\theta_1)\ rotx(\theta_2)\ rotx(\theta_3)$$
$$^{3}T_6 = {}^{I}T_3^T R$$
$$\theta_4 = \text{atan2}\left({}^3T_{6(1,2)},\ {}^3T_{6(3,2)}\right)$$
$$\theta_5 = \text{atan2}\left({}^3T_{6(3,2)}/c_4,\ {}^3T_{6(2,2)}\right)$$
$$\theta_6 = \text{atan2}\left({}^3T_{6(2,1)},\ \ -{}^3T_{6(2,3)}\right)$$

5.6 Equations of Motion

Given robot dynamics described by $H(\gamma)\ddot{\gamma} + d(\gamma, \dot{\gamma}) + G(\gamma) = F_\gamma$, the equations of motion for the manipulator can be determined. Solving this equation for the acceleration, $\ddot{\gamma}$, gives:

$$\ddot{\gamma} = H(\gamma)^{-1}\left(F_\gamma - d(\gamma, \dot{\gamma}) - G(\gamma)\right) \tag{1}$$

Where H is the system mass matrix, F_γ is the vector of generalized forces, d is the vector of centripital and coriolis effects, and G is gravitational effects.

$$H(\gamma) = \sum_{B}^{N} J_B(\gamma)^T \begin{bmatrix} {}_B^BJ & \mathring{S}({}_B^B\Gamma)^I T_B^T \\ {}^IT_B\mathring{S}({}_B^B\Gamma)^T & m_B I \end{bmatrix} J_B(\gamma)\ , \quad {}_B^B\Gamma =_B^B r_{cm} m_b\ , \quad \mathring{S}(\omega)r = (\omega \times r)$$

$$d(\gamma, \dot{\gamma}) = \sum_{B}^{N} J_B(\gamma)^T \begin{bmatrix} {}_B^BJ & \mathring{S}({}_B^B\Gamma)^I T_B^T \\ {}^IT_B\mathring{S}({}_B^B\Gamma)^T & m_B I \end{bmatrix} \dot{J}_B(\gamma, \dot{\gamma})\dot{\gamma} + J_B(\gamma)^T \begin{bmatrix} {}_B^B\omega_I \times_B^B J_B^B \omega_I \\ {}^IT_B\left({}_B^B\omega_I \times ({}_B^B\omega_I \times_B^B \Gamma)\right) \end{bmatrix}$$

$$G(\gamma) = \left(\frac{\partial U({}^Ir(\gamma))}{\partial \gamma}\right)^T \quad , \quad U_B = \begin{bmatrix} 0 & 0 & g \end{bmatrix}\left({}_B^I r_B m_B +^I T_B {}_B^B\Gamma\right)$$

Where J_B is the jacobian of the body, Γ is the vector of first mass moments, m_B is the mass of the body, and ${}_B^B\omega_I$ is the rotational velocity of the body relative to the inertial frame.

5.6.1 Actuator Dynamics

Given robot dynamics described by $H(\gamma)\ddot{\gamma} + n(\gamma, \dot{\gamma}) = \tau$, the torque, τ, provided by the servo motors is necessary to solve the closed loop dynamics of the system. Assuming the servo is driven by a D.C. motor with proportional derivative control,

$$\tau_a = Ki_a = J_a\ddot{\theta}_a + b_a\dot{\theta}_a + \tau_L \tag{2}$$

Where τ_a is the actuator torque, K is the back-EMF constant, i_a is the motor current, J_a is the armature inertia, θ_a, $\dot{\theta}_a, \ddot{\theta}_a$ is the motor position and it's first and second time derivatives respectively, b_a is the viscous friction coefficient, and τ_L is the torque available for the actuator to do work. The basic equation for a motor is known to be:

$$V_a = i_a R_a + K\dot{\theta}_a \tag{3}$$

Where V_a is the voltage applied to the actuator and R_a is the armature resistance. Given a gearbox with in/out ratio N and efficiency η,

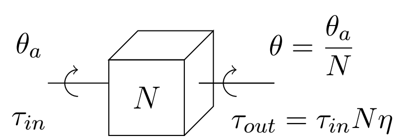

The motor equation (2) can be expressed in the output coordinates:

$$K i_a = J_a N \ddot{\theta} + b_a N \dot{\theta} + \frac{\tau}{N\eta}$$

Substituing into equation (3) and solving for i_a:

$$i_a = \frac{J_a N}{K}\ddot{\theta} + b_a N \dot{\theta} + \frac{\tau}{N\eta}$$

$$V_a = \frac{R_a J_a N}{K}\ddot{\theta} + \frac{R_a b_a N}{K}\dot{\theta} + \frac{R_a}{K N \eta}\tau + K N \dot{\theta} \tag{4}$$

Assuming PD control, $V_a = K_p(\theta - \theta_d) + K_d\dot{\theta}$, where θ_d is the desired orientation of the actuator, the following solution is found by setting the PD solution equal to (4). After collecting like terms:

$$\frac{R_a J_a N}{K}\ddot{\theta} + \left(\frac{R_a J_a N}{K} - K_d + KN\right)\dot{\theta} - K_p\theta = -K_p\theta_d - \frac{R_a}{KN\eta}\tau \tag{5}$$

The following parameters of the system can be obtained by applying a step input to the system with $\tau = 0$ and measuring the characteristics of it's response. Denoting ζ as the damping ratio and ω_n as the natural frequency of the system,

$$\%\text{ Overshoot} = \left(\frac{\theta_{max} - \theta_{ss}}{\theta_{ss}}\right) \times 100\ , \quad \zeta = \frac{-\ln(\%\text{OS}/100)}{\sqrt{\pi^2 + \ln^2(\%\text{OS}/100)}}\ , \quad \omega_n = \frac{\pi}{T_p\sqrt{1-\zeta^2}}$$

Given θ_{max}, θ_{ss}, and T_p as measured parameters of the system's max output, steady state, and time to peak, respectively.

Refactoring equation (5) and equating with the general solution for a second order system given by $\ddot{\theta} + 2\zeta\omega_n\dot{\theta} + \omega_n^2\theta = \omega_n^2\theta_d$, the following solutions are found:

$$2\zeta\omega_n = \frac{b_a}{J_a} - \frac{KK_d}{R_aJ_aN} + \frac{K^2}{R_aJ_a} \qquad (6) \qquad\qquad \omega_n^2 = \frac{-KK_p}{R_aJ_aN} \qquad (7)$$

Performing a similar experiment as previously described, except with a known inertial load $\tau = J_m\ddot{\theta}$, the following parameters can be found:

$$\alpha_m \equiv 2\zeta\omega_n = \frac{R_ab_aN^2\eta - KK_dN\eta + K^2N^2\eta}{R_aJ_aN^2\eta + R_aJ_m}\ , \quad \beta_m \equiv \omega_n = -\frac{KK_pN\eta}{R_aJ_aN^2\eta + R_aJ_m}$$

$$\begin{bmatrix} 1 & -(\alpha_1J_1 + \beta_1J_1) \\ 1 & -(\alpha_2J_2 + \beta_2J_2) \\ \vdots & \vdots \end{bmatrix} \begin{bmatrix} \dfrac{R_ab_aN^2\eta - KK_dN\eta + K^2N^2\eta - KK_pN\eta}{R_aJ_aN^2\eta} \\ \\ \dfrac{1}{J_aN^2\eta} \end{bmatrix} = \begin{bmatrix} \alpha_1 + \beta_1 \\ \alpha_2 + \beta_2 \\ \vdots \end{bmatrix} \qquad (8)$$

With multiple datasets (varying inertial loads, J_m), the solutions of (8) can be found using the least-squares method, yeilding

$$\frac{R_ab_aN - KK_d + K^2N\eta - KK_p}{R_aJ_aN} \qquad (9) \qquad\qquad \frac{1}{J_aN^2\eta} \qquad (10)$$

Finally, the coefficients of the second order system (11) are known:

$$\underbrace{\left(J_aN^2\eta\right)}_{1/(10)}\ddot{\theta} + \underbrace{\left(\frac{R_ab_aN^2\eta - KK_dN\eta + K^2N^2\eta}{R_a}\right)}_{(6)/(10)}\dot{\theta} - \underbrace{\left(\frac{KK_pN\eta}{R_a}\right)}_{(7)/(10)}\theta + \underbrace{\left(\frac{KK_pN\eta}{R_a}\right)}_{(7)/(10)}\theta_d = -\tau \quad (11)$$

The MATLAB code implementing this process can be found in the Appendix (see section 5.13, p. 39, *Listing 1*). The torque provided by the servo can now be solved for, given the current position (θ), velocity ($\dot{\theta}$), angular acceleration ($\ddot{\theta}$), and desired position (θ_d) are known.

Given the equation of motionfor the dynamical response of the system (1), substituting in the solution obtained for the motor dynamics and solving for the acceleration,

$$\left(H + J_aN^2\eta\right)^{-1}\left[\left(B - \frac{R_ab_aN^2\eta - KK_dN\eta + K^2N^2\eta}{R_a}\right)\dot{\gamma} - \left(\frac{KK_pN\eta}{R_a}\right)(\gamma_d - \gamma) - n\right] = \ddot{\gamma} \qquad (12)$$

Where

$$n(\gamma,\dot{\gamma}) = d(\gamma,\dot{\gamma}) + G(\gamma) + C\mathrm{sgn}(\dot{\gamma})$$

5.7 Open-Loop Simulation

The equations of motion described in equation (1) can be integrated to simulate the motion of the system. For the open loop control, no input torque is supplied, meaning the system responds only to gravity. Due to the complexity of the equations of motion, they will be integrated numerically using a 4th Order Runge-Kutta method algorithm [1]. Since no input force is supplied, the equations of motion reduce down to the relation described in equation (13).

$$\ddot{\gamma} = H(\gamma)^{-1}(-d(\gamma, \dot{\gamma}) - G(\gamma)) \tag{13}$$

The resulting simulation shows the manipulator assembly starting in the zeroed configuration, (*Figure 15a*) then "falling" due to the forces of gravity acting on the links (*Figure 15b*). The manipulator continues to oscillate analogous to a simple pendulum, being that there are no frictional forces accounted for.

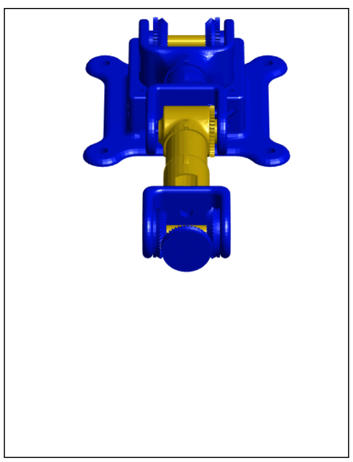

(a) Frame Snapshot near Simulation Initiation

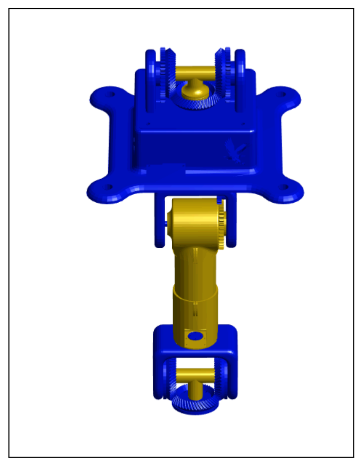

(b) Frame Snapshot near Simulation Termination

Figure 15: Open-Loop Control Simulation Animation Snapshots

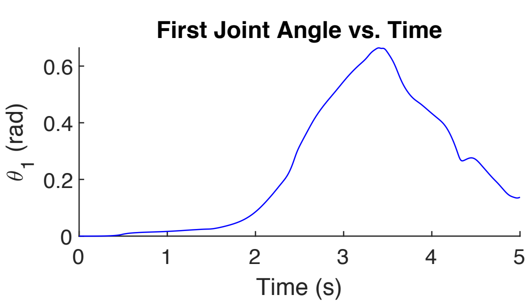

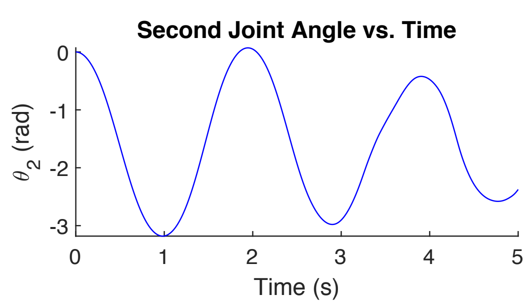

Figure 16: Joint Angles vs Time in Open-Loop Simulation

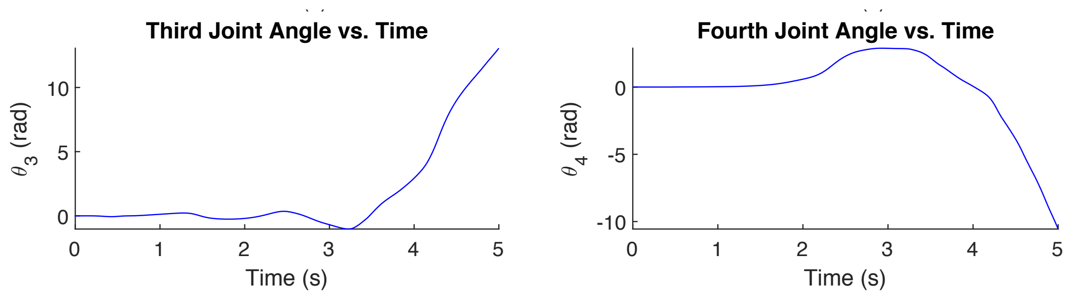

Figure 17: Joint Angles vs Time in Open-Loop Simulation

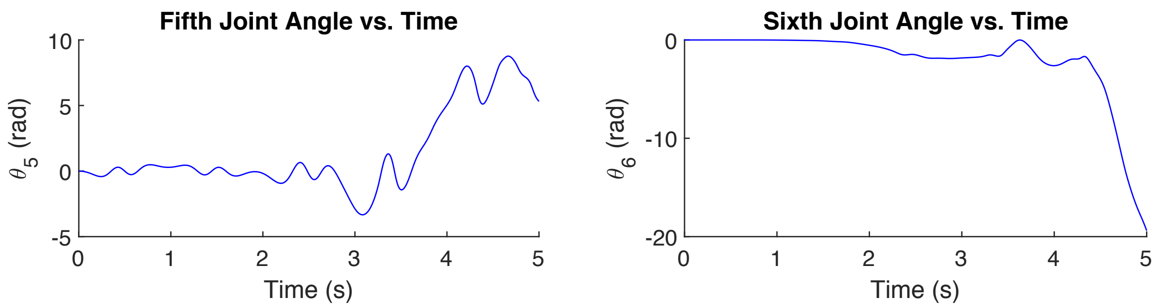

Figure 18: Joint Angles vs Time in Open-Loop Simulation

5.8 Closed-Loop Simulation

The motor equation (11) gives an expression for the motor torques, however the system dynamics are defined in terms of geometric joint angles. The inclusion of differential drive systems means that the joint angles, γ do not directly correspond to motor rotations, θ. However, there is a linear relation between them, described in equation (14).

$$\gamma = A\theta \quad \text{where} \quad A = \begin{bmatrix} 1/(2N) & 1/(2N) & 0 & 0 & 0 & 0 \\ 1/(2N) & -1/(2N) & 0 & 0 & 0 & 0 \\ 0 & 0 & -1/N & 0 & 0 & 0 \\ 0 & 0 & 0 & 1 & 0 & 0 \\ 0 & 0 & 0 & 0 & -1/2 & 1/2 \\ 0 & 0 & 0 & 0 & 1/2 & 1/2 \end{bmatrix} \tag{14}$$

Equation (14) can be used to map the joint angles to the motor angles. The gear ratio of 1:10 is represented by the variable N. Similarly, the motor angles can be determined by multiplying both sides of equation (14) by the inverse of matrix A, giving the following relation.

$$\theta = A^{-1}\gamma \tag{15}$$

It is important to note that the virtual work done by the joint torques (F_γ) and the virtual work done by the motor torques (F_θ) are equal. Using equation (15), a linear relation between the joint torques and motor torques can be determined.

$$\begin{aligned}
\delta W = F_\theta^T \delta\theta &= F_\gamma^T \delta\gamma, \text{ where } \delta\gamma = A\delta\theta \\
F_\theta^T \delta\theta &= F_\gamma^T (A\delta\theta) \\
F_\theta^T &= F_\gamma^T A \\
\left(F_\theta^T\right)^T &= \left(F_\gamma^T A\right)^T \\
F_\theta = A^T F_\gamma &\Leftrightarrow F_\gamma = A^{-T} F_\theta
\end{aligned}$$

Using this equation, a relation can be determined between the motor dynamics and the system dynamics given in equation (11) and equation (1) respectively.

$$\begin{aligned}
H(\gamma)\ddot{\gamma} + d(\gamma,\dot{\gamma}) + G(\gamma) &= -A^{-T}\left(C_1 A^{-1}\ddot{\gamma} + C_2 A^{-1}\dot{\gamma} + C_3\theta_d - C_3 A^{-1}\gamma\right) \\
\ddot{\gamma} = H(\gamma)^{-1}\Big(-A^{-T}&\left(C_1 A^{-1}\ddot{\gamma} + C_2 A^{-1}\dot{\gamma} + C_3\theta_d - C_3 A^{-1}\gamma\right) - d(\gamma,\dot{\gamma}) - G(\gamma)\Big) \qquad (16)
\end{aligned}$$

Because this equation includes the motor model, which in turn includes an internal PD controller, this equation can be integrated to solve for the system response given a desired motor angle input, θ_d. However, doing so will not result in the desired system response. This control scheme does not have any compensation for the inertia of the links, and it is also lacking gravity compensation. This can be remedied by modifying the input to the motors, θ_d. A new input, u, is defined such that gravity can be compensated. Thus, the motor input term in equation (16) must include both compensation for gravity and the desired motor angle.

$$\begin{aligned}
A^{-T} C_3 u &= G(\gamma) + d(\gamma,\dot{\gamma}) + A^{-T} C_3 \theta_d \\
u &= \left(A^{-T} C_3\right)^{-1} G(\gamma) + \theta_d \qquad (17)
\end{aligned}$$

With this new motor input, the closed loop control system equations of motion are given as:

$$\ddot{\gamma} = H(\gamma)^{-1}\left(-A^{-T}\left(C_1 A^{-1}\ddot{\gamma} + C_2 A^{-1}\dot{\gamma} + C_3 u - C_3 A^{-1}\gamma\right) - d(\gamma,\dot{\gamma}) - G(\gamma)\right) \qquad (18)$$

Equation (18) can then be integrated to solve for the system response given desired motor angles.

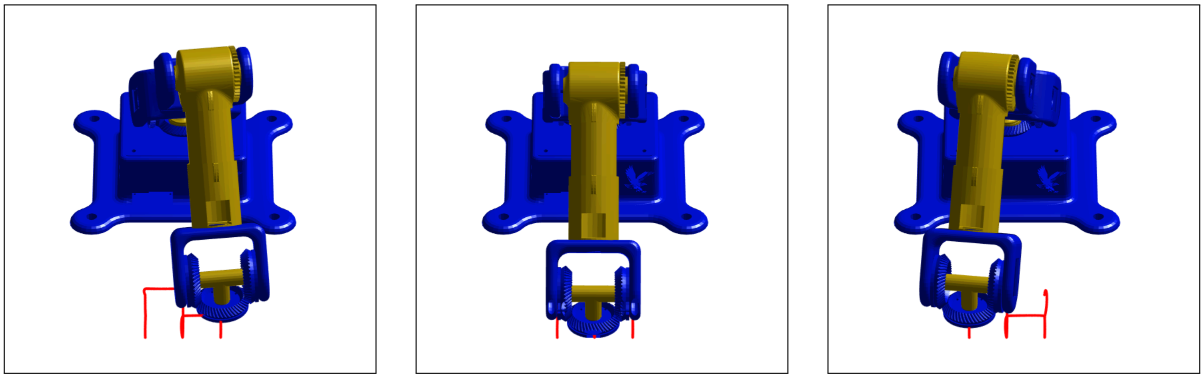

(a) Frame Snapshot near Simulation Initiation

(b) Frame Snapshot near Simulation Middle

(c) Frame Snapshot near Simulation Termination

Figure 19: Closed-Loop Control Simulation Animation Snapshots

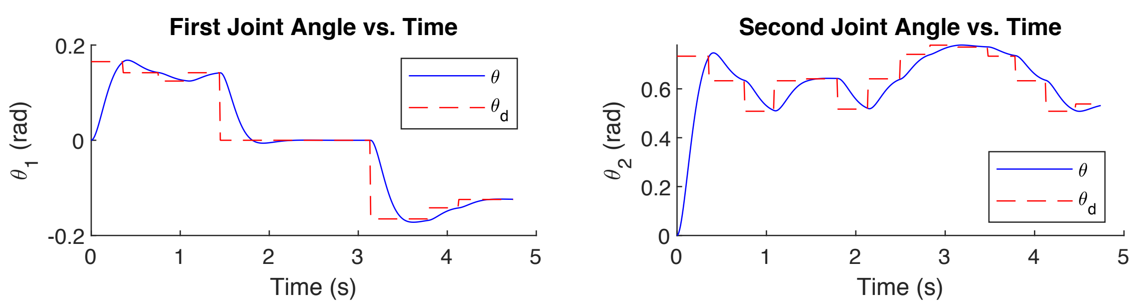

Figure 20: Joint Angles vs Time in Closed-Loop Simulation

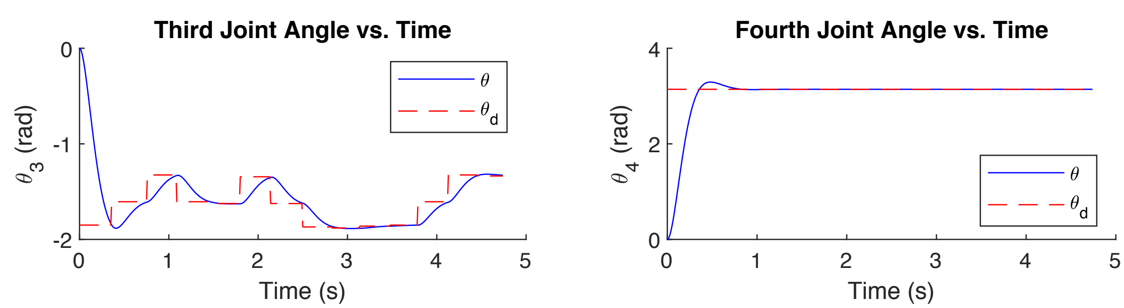

Figure 21: Joint Angles vs Time in Closed-Loop Simulation

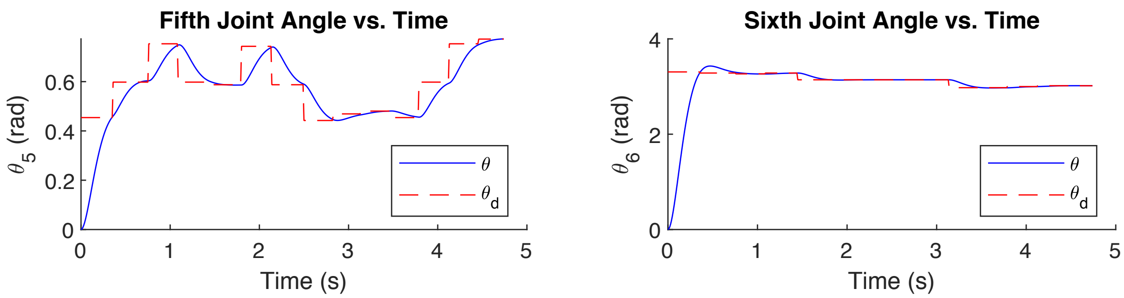

Figure 22: Joint Angles vs Time in Closed-Loop Simulation

5.9 ANSYS

With 100% infill, 3D printed PLA has a maximum shear stress of 13.6 kpsi. The manipulator applies a load of 13N in the negative y-direction. Without gears in the base differential, the differential support would bear the load on its bearing mounts. *Figure 23* shows the manipulator's differential support could experience up to 97 kPa or 0.014 kpsi of shear stress, which is less than the maximum shear stress of PLA with 100% infill. Since some of the manipulator's mass is supported by the gears, the actual shear experienced by the differential support will be less.

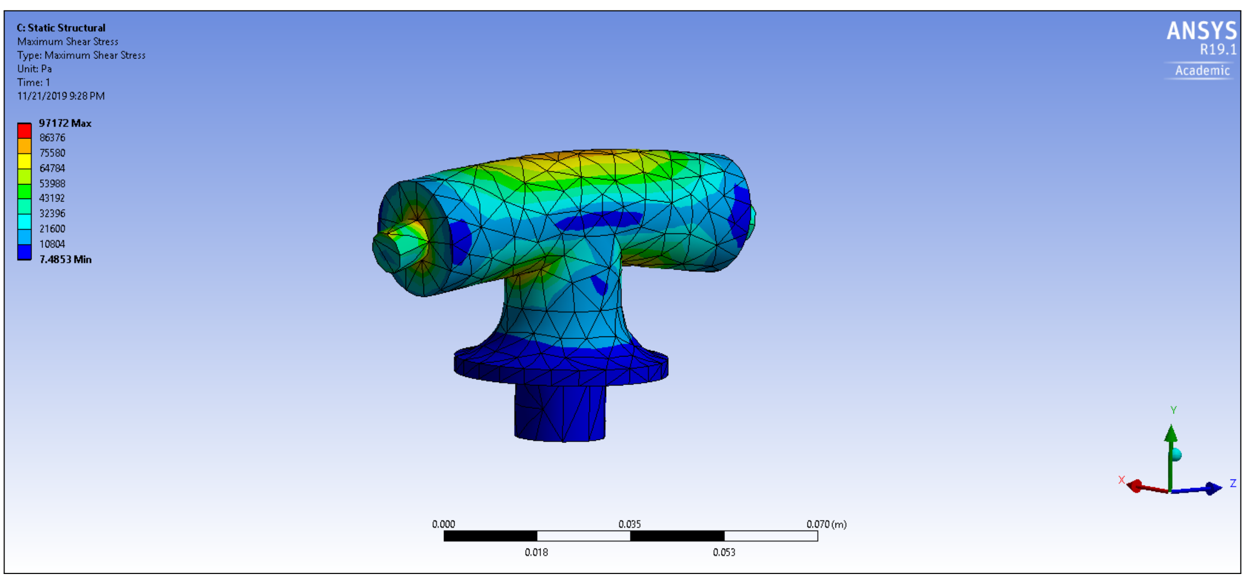

Figure 23: T-Bar ANSYS FEA

To simulate a dynamical loading situation where the manipulator would be under the largest amount of stress, gravitational forces and an outward force (parallel to the arm direction in it's zeroed configuration) were applied to the structure. This situation represents the worst-case loading scenario, such as the manipulator swinging while outstretched. The supports and simulated forces can be seen in the ANSYS image capture shown in *Figure 24*.

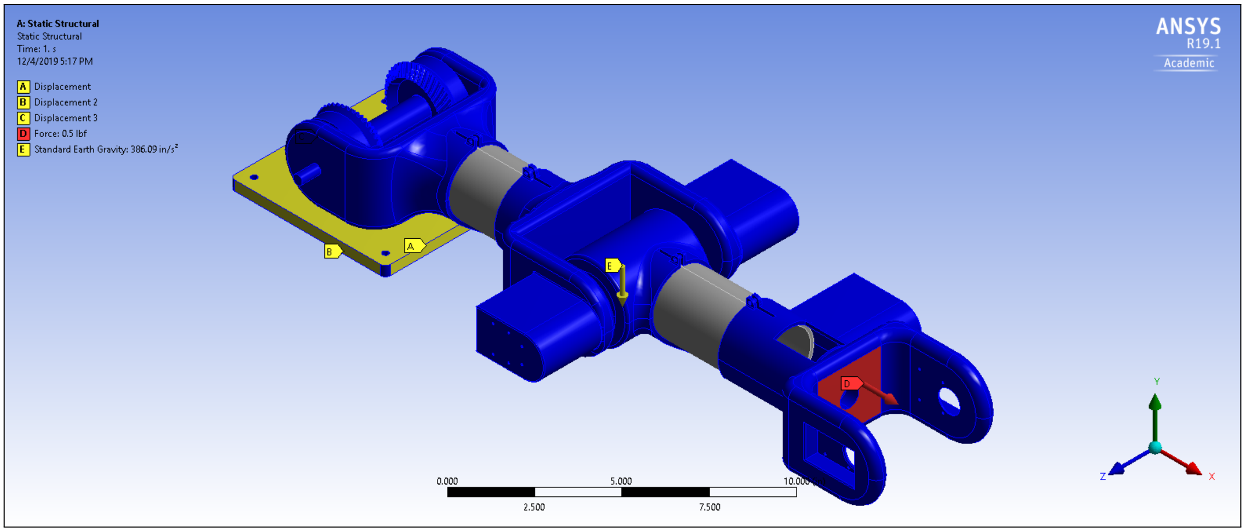

Figure 24: ANSYS Simulated Forces Image Capture

As shown in *Figure 24*, the red arrow is the outward force simulating centrifugal forces, the yellow arrow represents gravity acting at the manipulator's center of mass, and the yellow highlighted faces show the fixed support at the base.

The dynamical loadings resulted in a maximum shear stress at the shoulder differential bearing, as seen in *Figure 25a*; a close-up image of the bearing analysis can be seen in *Figure 25b*.

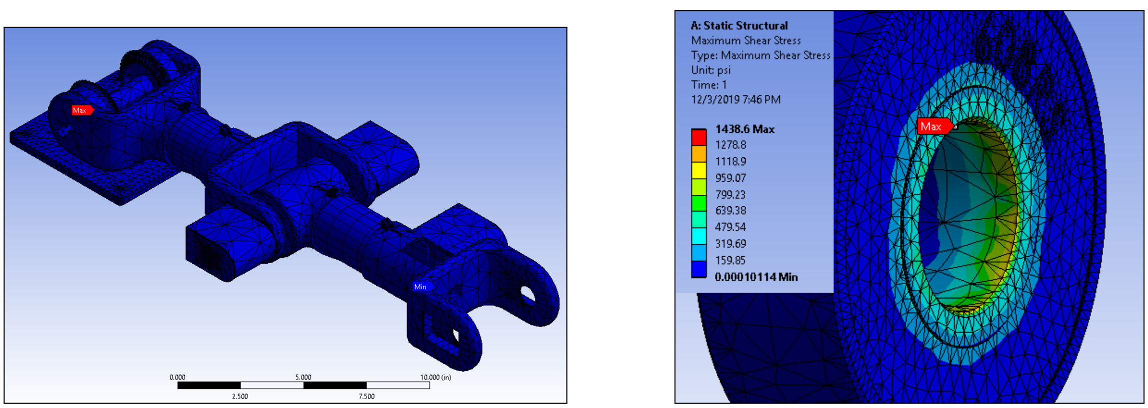

(a) ANSYS Full View of Maximum Shear (b) ANSYS Bearing Shear Stress Close-up

Figure 25: ANSYS FEA of Dynamical Loading Scenario

To further validate that the structure is capable of handling alternating stresses, a fatigue test was also performed showing the life of the manipulator handles a minimum of 1e6 cycles, as seen in *Figure 26*, showing it is unlikely to fail due to material yeilding.

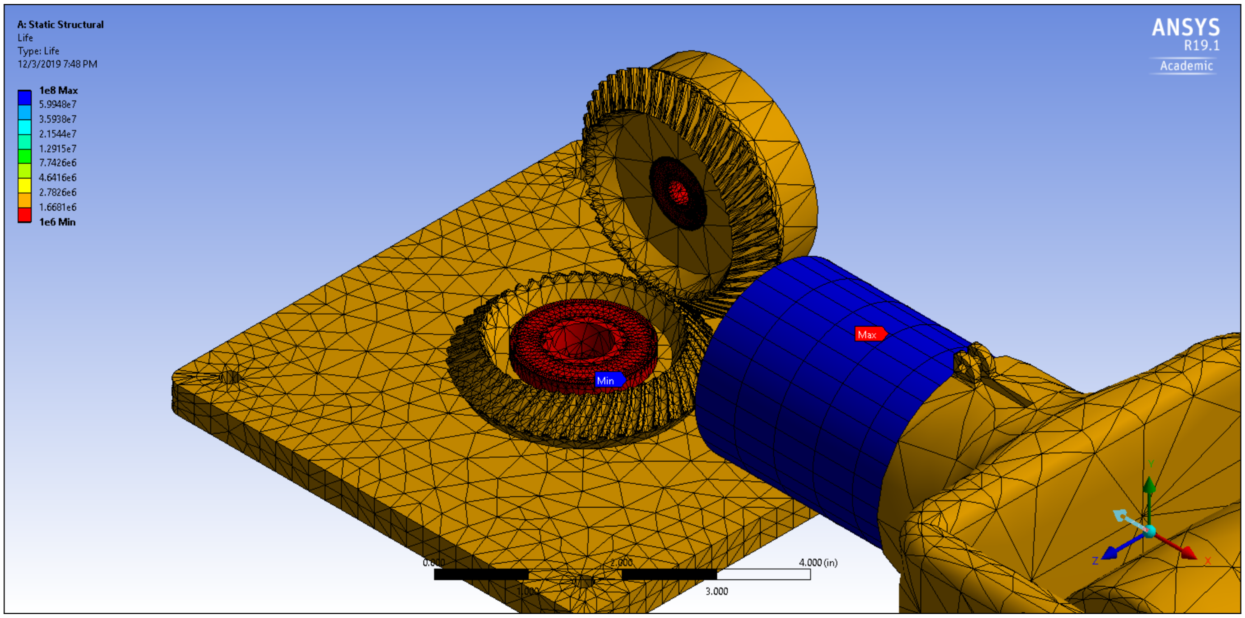

Figure 26: ANSYS Fatigue Test

As seen in *Figure 26*, the lower bearing of the differential drive on the shoulder of the manipulator would be the most likely component to fail under repeating loadings.

5.10 Electrical Schematic

The electrical schematic shown in *Figure 27* consists of a power supply that receives 120V AC that is standardly supplied from wall outlets. The Power supply has two outputs, a 5V terminal that has a max current output of 3A, and a 12V terminal that has a max output of 7A. The Raspberry Pi 3B is powered by the 5V terminal, and since the max current draw from the Pi is 1.2A the maximum current draw from the terminal is not surpassed. The six MX-12W servos used in the manipulator, as well as the AX-12A servo used in the end effector, are connected in parallel across the 12V terminal from the power supply. Since the MX-12W has a stall current of .6A and the AX-12A has a stall current of 1.5A, the maximum current to be pulled from the 12V terminal would be 5.1A, less than the 7A the supply can output. In order to communicate to the servos, a U2D2 communication converter is connected to the Raspberry Pi which creates a serial connection used by the servos, allowing the servos to be daisy-chained together. The Raspberry Pi also connects to an external PC so that the user can communicate with the Pi using a mouse, keyboard, and monitor.

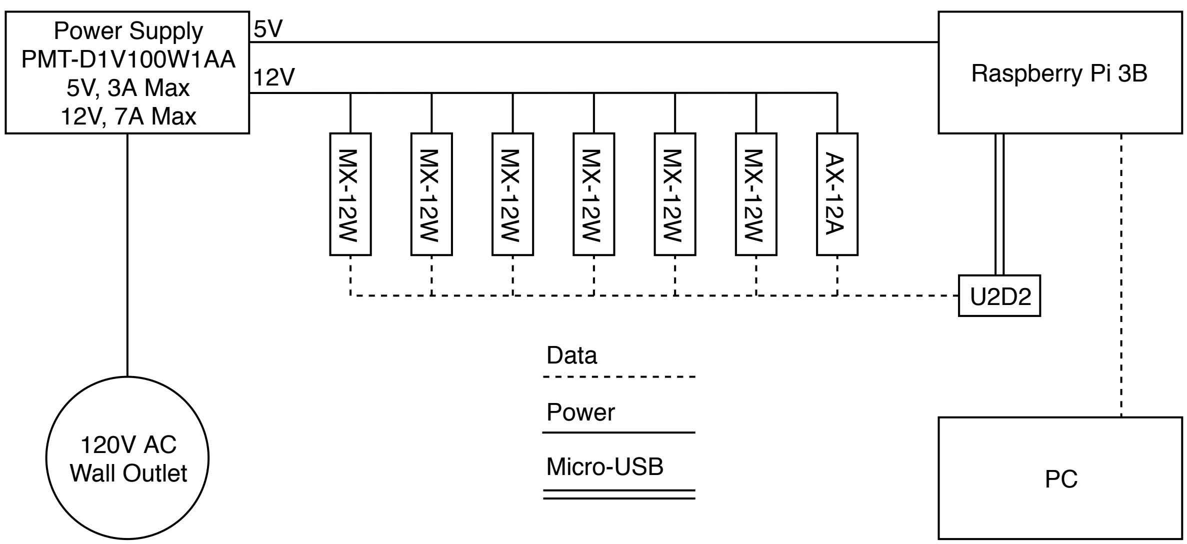

Figure 27: Electrical Schematic

5.11 Software Flowchart

The software the system uses takes in a row vector of position, orientation, path type, and end effector function information for all points to be traveled through and runs the manipulator through the desired points following the specified paths requested. The general overview of the code is shown in *Figure 28*. *Figure 28* shows that the software for the manipulator is broken up into six subsections, two sections that receive data, three that do calculations, and one that runs the specified task.

The first subsection of the software works to receive the number of points the user is inputting as well as the general task the user is completing, shown in *Figure 29*. *Figure 29* specifies that the software prompts the user for the number of points that the manipulator will travel

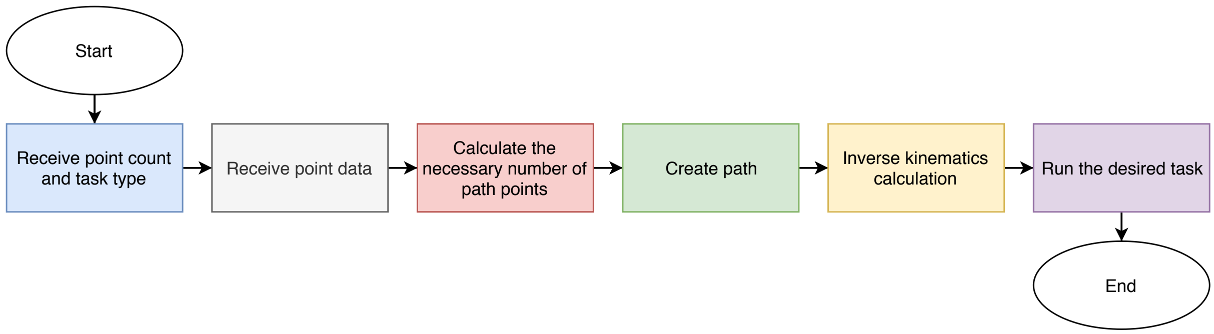

Figure 28: General Software Algorithm Overview

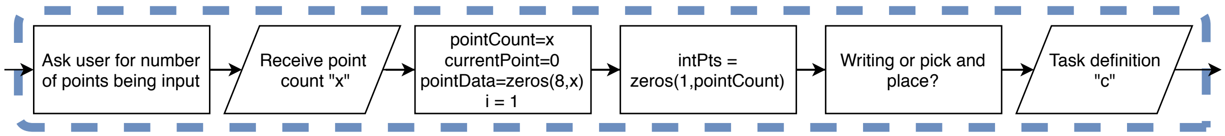

Figure 29: Software Flowchart Subsection 1

through and stores the input as a variable, in this case ‘x’. The ‘x’ variable is only used to help preallocate data vectors so that the size of the vector does not change with each input. The software also receives the task specification as either a 0 for cartesian straight line pathing or a 1 for a straight line in the joint space and stores this value in the variable ‘c’.

The second general block in the software flowchart works to receive and store the necessary data for the points the user is inputting depending on the path type as seen in *Figure 30*.

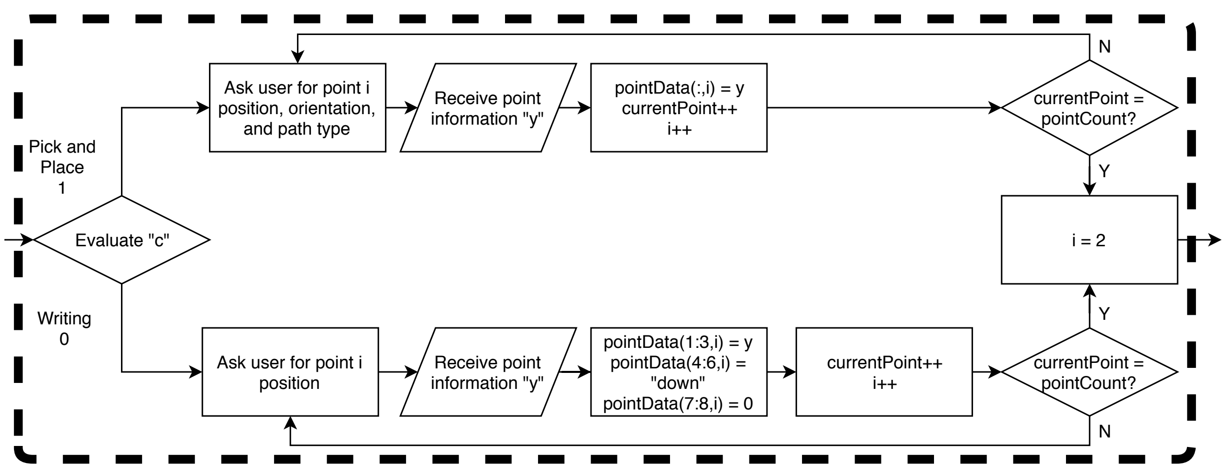

Figure 30: Software Flowchart Subsection 2

Figure 30 shows that the path type variable 'c' is used to determine what information is necessary to collect. If the user is doing a writing task, the software only collects the x, y, and z distances for the point and assumes that the end effector orientation will be facing down so that the marker is vertical. If the user is doing pick and place, the software prompts the user for the x, y, z, phi, theta, psi, path type, and end effector data. The software loops until all the points have been input.

The next block in the software flowchart calculates the total points necessary to complete the task. The overview for this section can be seen in *Figure 31*.

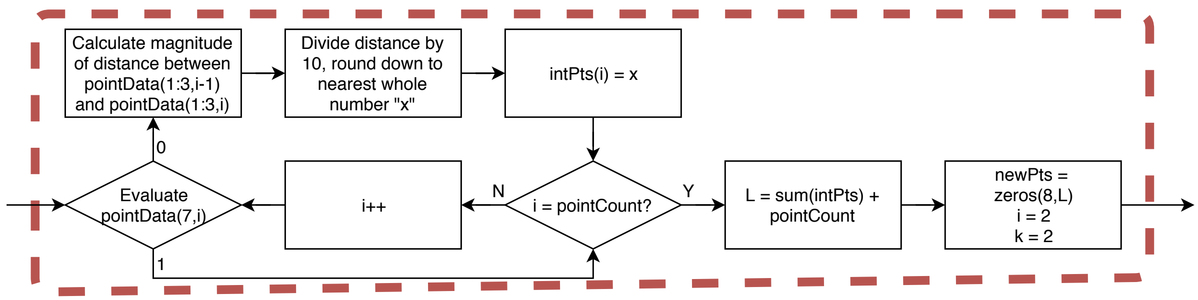

Figure 31: Software Flowchart Subsection 3

As seen in *Figure 31*, the section of software calculates the distance between the current point and the previous point if the path type is cartesian straight line and divides the distance by ten to find the number of centimeters between the two points. This value is stored as the necessary number of intermediate points, and the software will loop through until every point has been checked. The section of code also stores the total number of points that will be used as the variable level for later use.

The fourth code block in the flowchart creates and stores the necessary intermediate points along the desired path, shown in *Figure 32*.

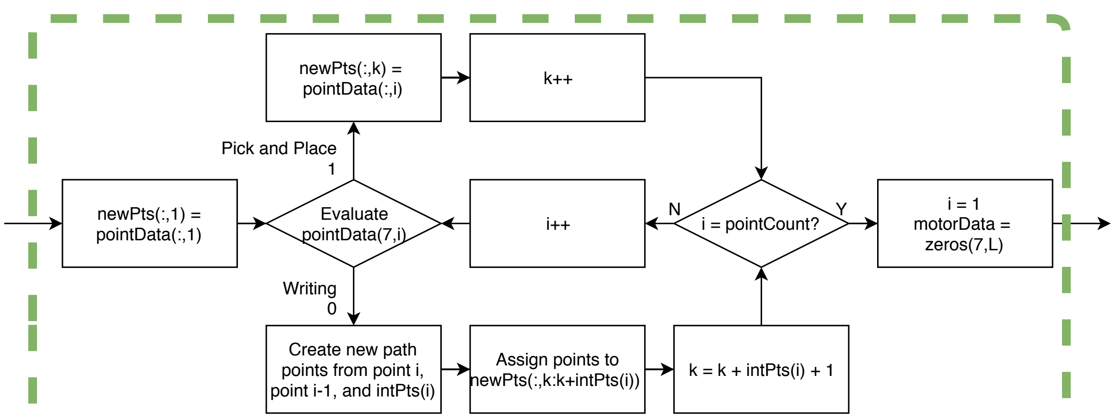

Figure 32: Software Flowchart Subsection 4

The code shown in *Figure 32* creates points every centimeter if the path type is cartesian straight line using the number of path points stored for each point from the previous block of software. This ensures that a straight line will be followed between the two user input points. If the path type is a straight line in the joint space, the software does not add any intermediate points since the path seen in the cartesian space does not matter.

The fifth code block in the flowchart calculates inverse kinematics of the points defined in the previous block of code and stores the angles as counts that can be used by the servos. The overview of this section can be seen in *Figure 33*.

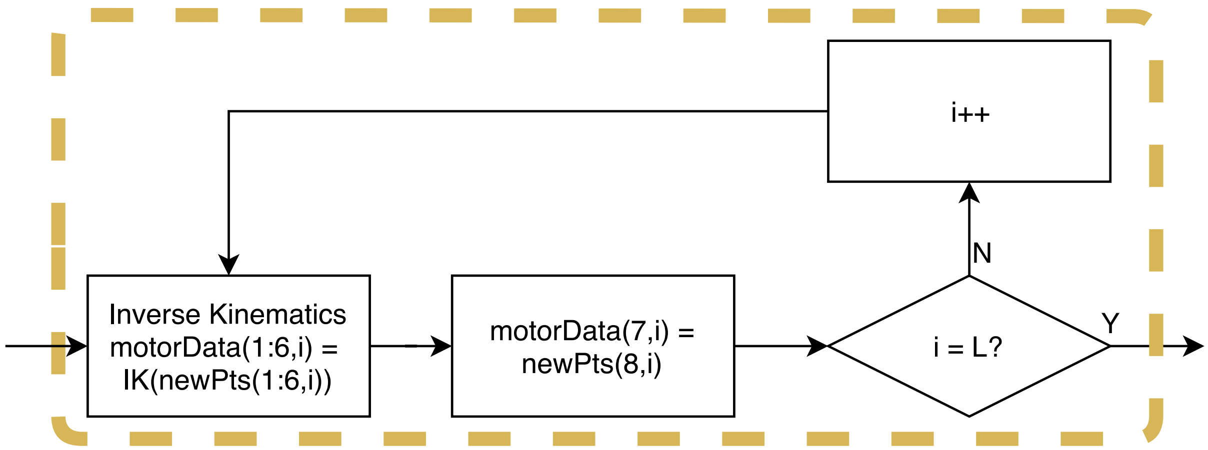

Figure 33: Software Flowchart Subsection 5

Figure 33 shows that the new points found in the prior section of code are run through an inverse kinematics function that will output the necessary counts the servos can utilize. The code iterates through each point until the inverse kinematics have been calculated for all points.

The final block in the software diagram runs the manipulator through the desired task, with this section of code requiring user input at certain stages depending on the path type, seen in *Figure 34*.

The code in *Figure 34* prompts the user to press space to close the end effector and grab the marker if drawing was the specified task, otherwise the software jumps straight into prompting the user to begin the task, and when the user begins the task the counts for each position are sent to the servos one at a time. The counts for the next position are not sent to the servos until the servos have reached the desired positions and the end effector function has been completed if there is one.

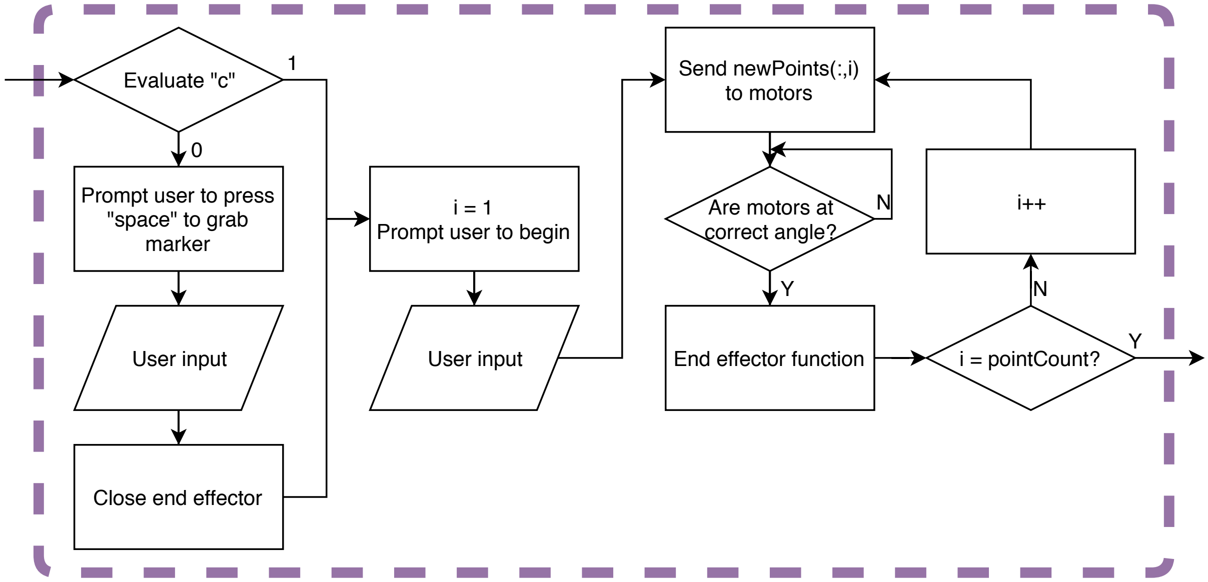

Figure 34: Software Flowchart Subsection 6

5.12 Project Status and Future

— Print Differential

— Cut Aluminum Supports

— Print Base

— Print Link 1

— Test Link 1 and Differential

— Print Differential Support

— Test Differential

— Test Link 1 Pulleys

— Test Link 1 with Motors

— Test Motor Control of Differential

— Test Link 1 With Load

— Implement Kinematics in Python

— Test Kinemtics with Motors

5.13 Parts List

Table 3 lists the parts MEIOSIS will require to build the manipulator. The total cost is $629.22 including shipping. Specification 1.1b required MEIOSOS's cost to develop the manipulator be less than $800. In addition to pulley belts for the current configuration, *Table 3* allocates $20 for two additional belt sizes to increase joint 1/2's and joint 3's torque by a factor of 10. One belt size and the belt must be purchased in packs of 3 from Automation Direct. *Table 3* accounts for increased cable lengths of 500 mm to communication bus signals from motor 2 to 3 and motor 3 to 4 and 350 mm to communication bus signals from motor 5 to 6. Motors are identified in [ZACK'S FIGURE]. Aside from electronic hardware, Figure ZZ accounts for physical hardware: To 100 threaded press-fit inserts. The manipulator will require between 21 and 46 inserts. The majority of inserts attach MX-12W servos to the manipulator. Mounting hardware accompanies each servo.

Table 3: MEIOSIS Bill of Materials with Costs

Part	Retailer	Quantity	Unit Cost (USD)	Total Cost (USD)
3 pack, 300 tooth	Automation Direct	1	11.5	11.5
3 pack, 208 tooth		1	9.5	28.5
Base second belts		1	10	10
Link 3 second belts		1	10	10
MX-12W	Trossen Robotics	6	65.9	395.4
500 mm, 1/2 pulleys		2	3.95	7.9
350 mm, 3 pulley		1	2.95	2.95
EE		1	24.95	24.95
Pi 3 B	Amazon	1	37.99	37.99
Bearings		1	8.99	8.99
2 Sch 10 12" Al tube	Industrial Metal Sales	1	2.99	2.99
12 V, 5 V power supply	Digi-Key Electronics	1	43.21	43.21
Automation Direct	Shipping	—	—	0
Trossen Robotics				13.15
Amazon				0
Industrial Metal Sales				26.36
Digi-Key				8.99
			Total	629.22

In addition to the costs listed in *Table 3*, *Table 4* shows all further costs for the end-user. Since the Embry-Riddle robotics lab has 3D printing available without affecting MEIOSIS's

$800 budget, *Table 4* accounts for outsourced 3D printing costs sufficient to print the entire manipulator with six sets of pulleys. If the end-user owns a 3D printer, the 3D printing cost would effectively reduce to filament cost. Additionally, *Table 4* assumes the end-user does not already possess an AX-12A servo to be used with the end-effector. Further, *Table 4* assumes the manipulator would be more accessible to end-users by using a proprietary U2D2 communication module in lieu of a soldered or bread-board circuit. The robotics lab has an AX-12A servo and U2D2 communication module MEIOSIS will use. With the aforementioned additional costs, the MEIOSIS manipulator costs the end-user $1,007.98 including shipping costs. While $1,007.98 is slightly above the maximum cost of $1000 from specification 1.1a, it provides greater accessibility, which may be diminished by assuming end-users posess 3D printers.

Table 4: End-User Bill of Materials with Costs

Part	**Retailer**	**Quantity**	**Unit Cost (USD)**	**Total Cost (USD)**
Aforementioned Costs	*Table 3*	—	—	629.22
U2D2	Trossen Robotics	1	49.9	49.9
EE with servo	Trossen Robotics	1	64.95	64.95
3D PLA outsourcing (incl. shipping)	Craft Cloud	1	288.86	288.86
			Total	1007.98

Acknowledgements & Attributions

We would like to acknowledge the following people for their contibutions in creating this report.

— Dr. Isenberg

— Dr. Schipper

References

[1] Michael Zeltkevic 1. Runge-kutta methods, 04 1998.

[2] S. Hutchinson M. Spong and M. Vidyasager. *Robot Modeling and Control*. 2006.

[3] ROBOTIS. Ax-12a e-manual, 2019.

A Appendix

A.I Relevant Figures and Materials

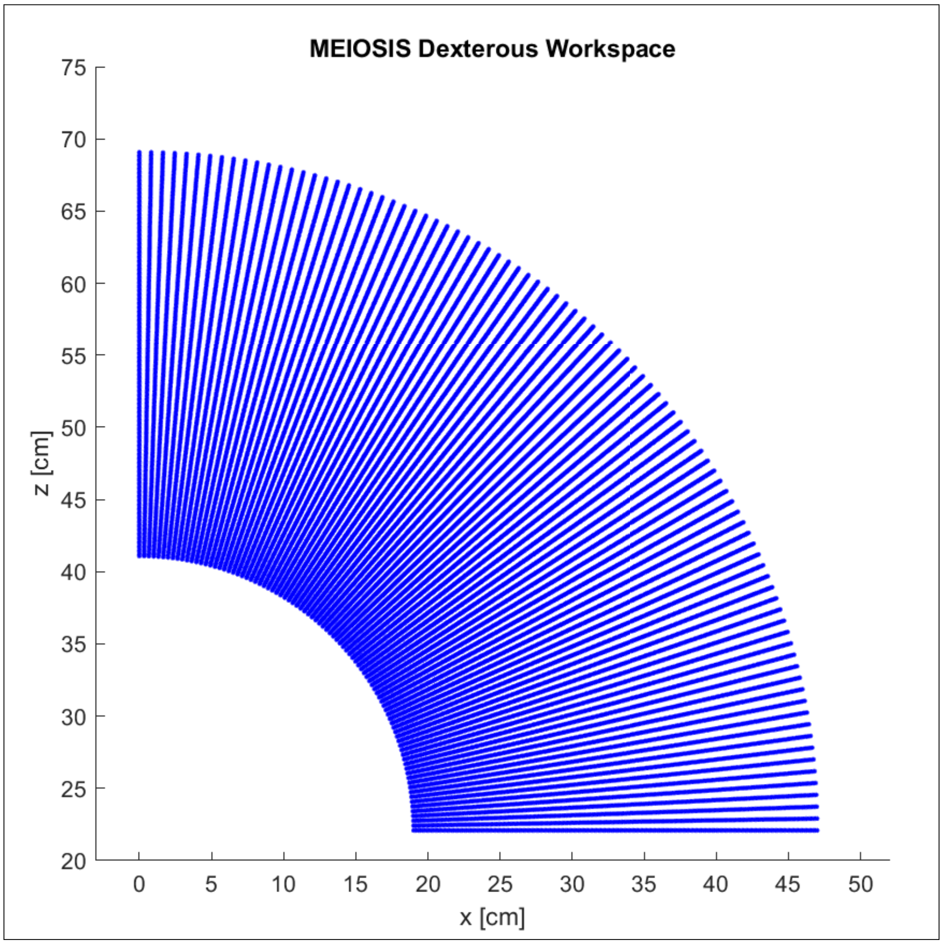

Figure 35: Cross Section of Dexterous Workspace Quadrant

A.II CAD Drawings

The complete drawing package is attached.

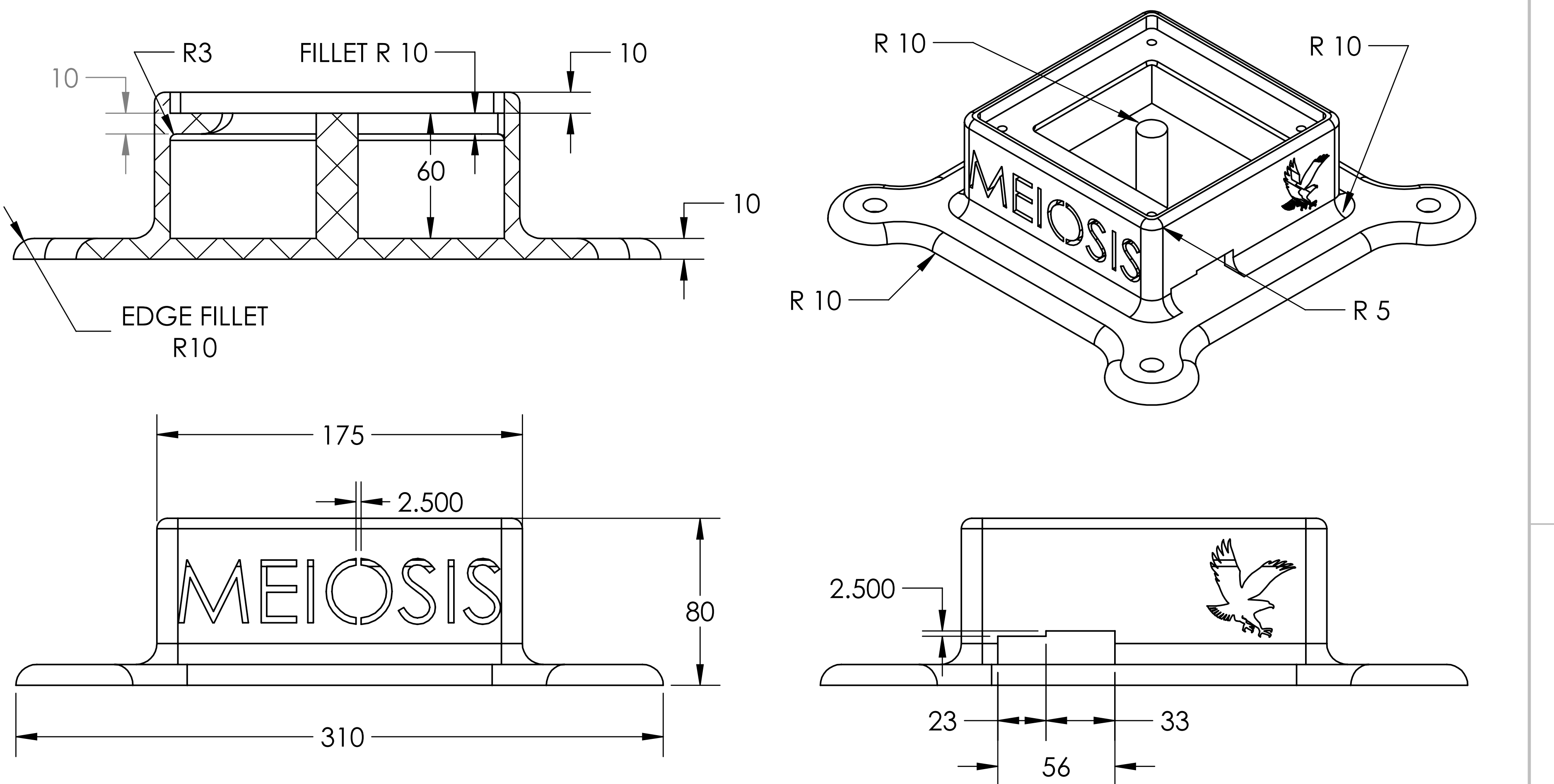

UNLESS OTHERWISE SPECIFIED:		NAME	DATE	
DIMENSIONS ARE IN MILLIMETERS TOLERANCES: ±3.0	DRAWN	Ryan W.	11/13/2019	
	CHECKED			TITLE: Base Bottom
	ENG APPR.			
	MFG APPR.			
INTERPRET GEOMETRIC TOLERANCING PER:	Q.A.			
MATERIAL PLA, 30% Infill	COMMENTS:			SIZE A DWG. NO. REV 1.0
FINISH N/A				
DO NOT SCALE DRAWING				SCALE: 1:5 · WEIGHT: · SHEET 1 OF 18

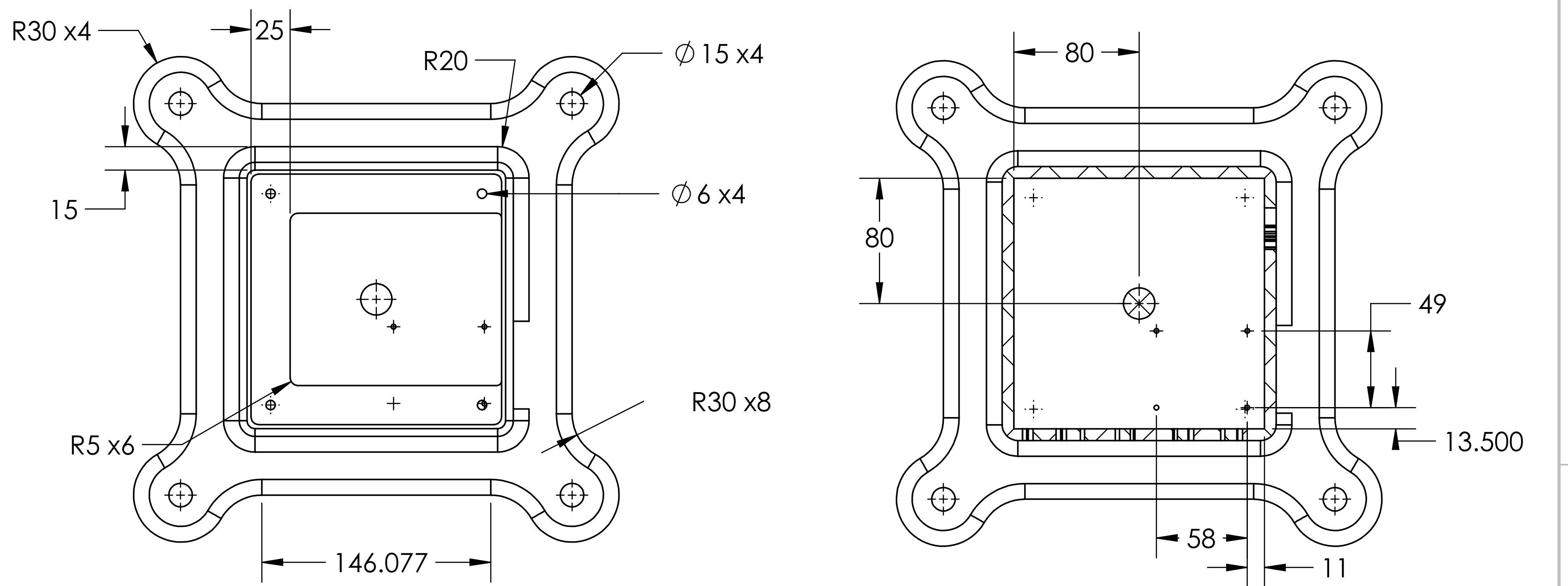

UNLESS OTHERWISE SPECIFIED:		NAME	DATE	
DIMENSIONS ARE IN MILLIMETERS	DRAWN	Ryan W.	11/13/2019	
TOLERANCES: ±3.0	CHECKED			TITLE: Base Bottom
	ENG APPR.			
	MFG APPR.			
INTERPRET GEOMETRIC TOLERANCING PER:	Q.A.			
MATERIAL PLA, 30% Infill	COMMENTS:			SIZE A
FINISH N/A				DWG. NO.
DO NOT SCALE DRAWING				REV 1.0
				SCALE: 1:5
				WEIGHT:
				SHEET 2 OF 18

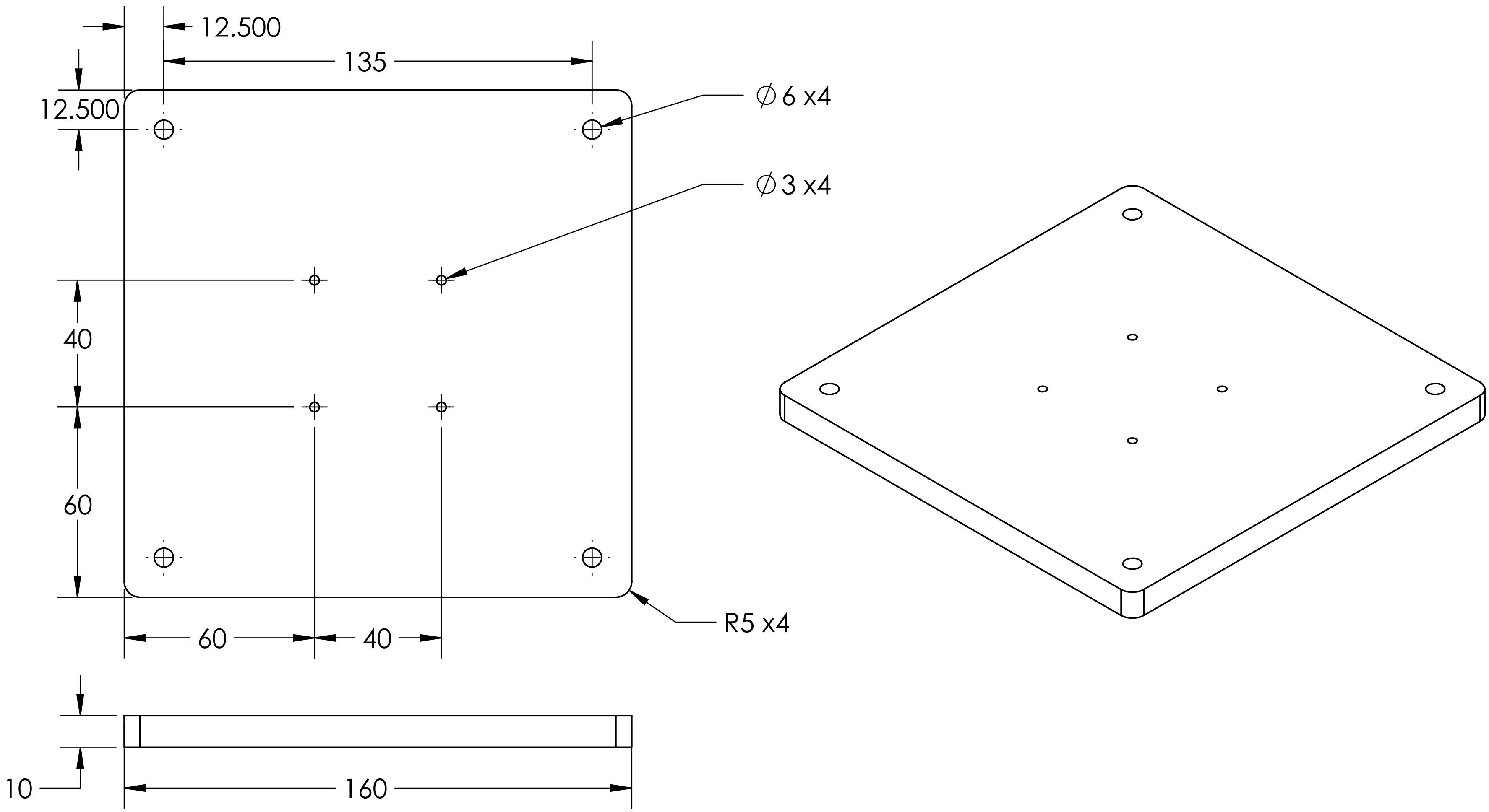

UNLESS OTHERWISE SPECIFIED:		NAME	DATE
DIMENSIONS ARE IN MILLIMETERS	DRAWN	Ryan W.	11/8/2019
TOLERANCES: ±3.0	CHECKED		
	ENG APPR.		
	MFG APPR.		
INTERPRET GEOMETRIC TOLERANCING PER:	Q.A.		
MATERIAL PLA, 30% Infill	COMMENTS:		
FINISH N/A			
DO NOT SCALE DRAWING			

TITLE:

Base Top

SIZE	DWG. NO.	REV
A		1.0
SCALE: 1:5	WEIGHT:	SHEET 3 OF 18

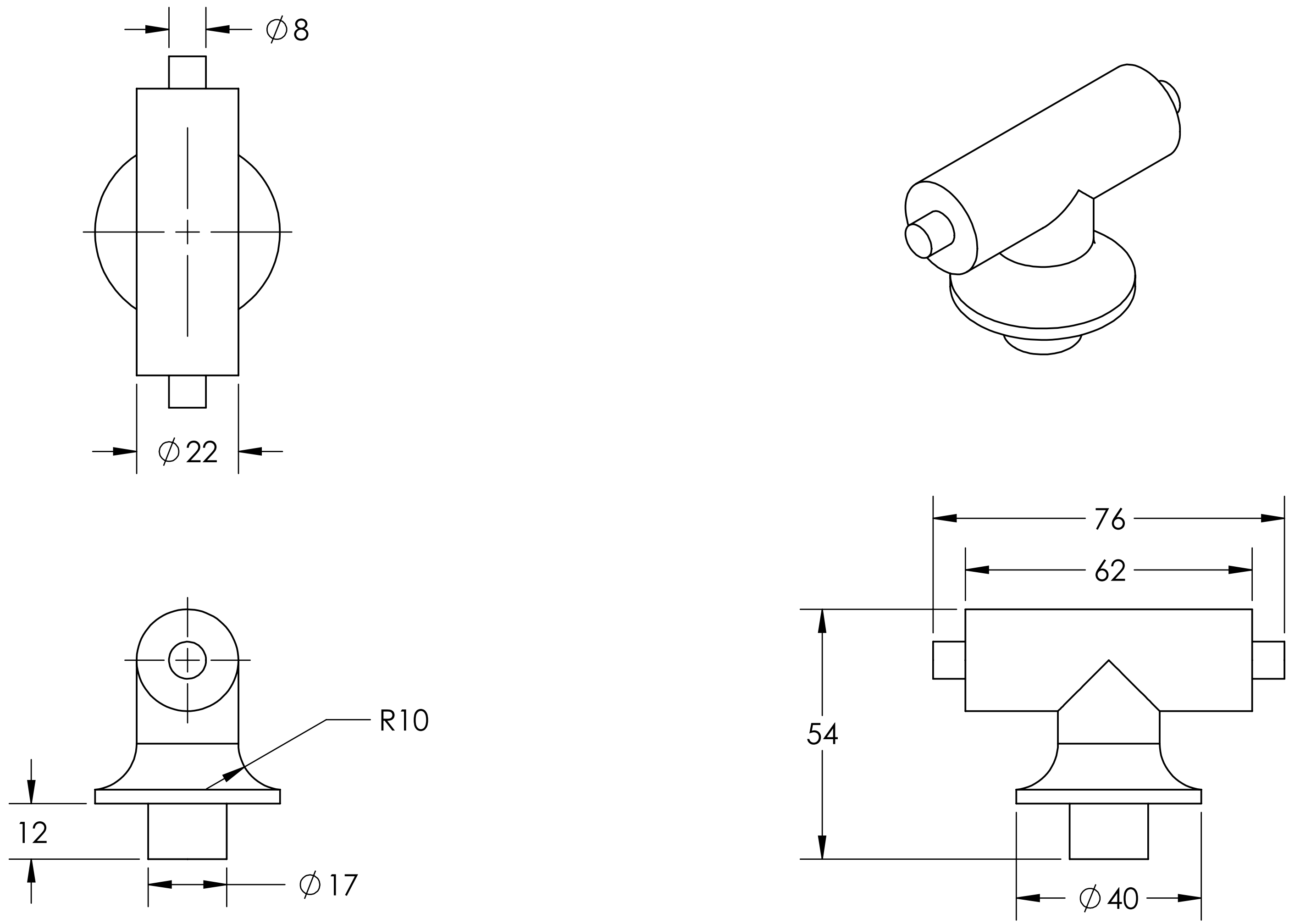

UNLESS OTHERWISE SPECIFIED:		NAME	DATE	
DIMENSIONS ARE IN MILLIMETERS	DRAWN	Ryan W.	11/8/2019	TITLE:
TOLERANCES: ±3.0	CHECKED			Shoulder Differential T-Bar
	ENG APPR.			
	MFG APPR.			
INTERPRET GEOMETRIC TOLERANCING PER:	Q.A.			
MATERIAL PLA, 30% Infill	COMMENTS:			SIZE A · DWG. NO. · REV 1.0
FINISH N/A				SCALE: 1:2 · WEIGHT: · SHEET 4 OF 18
DO NOT SCALE DRAWING				

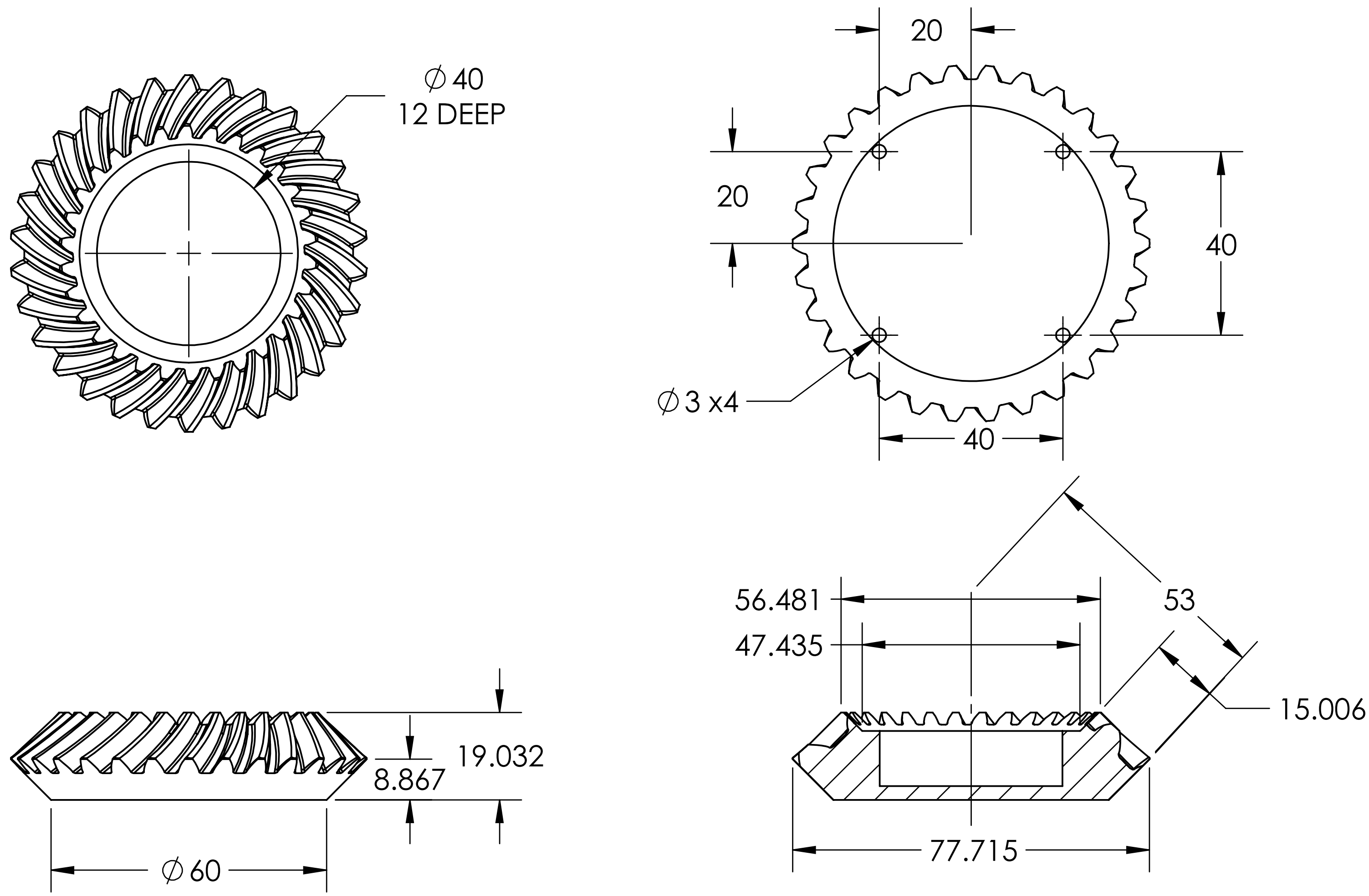

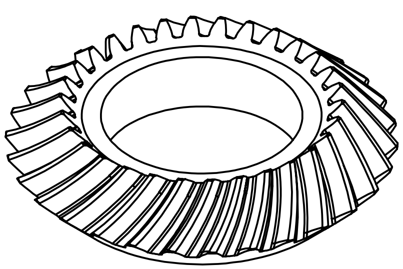

UNLESS OTHERWISE SPECIFIED:		NAME	DATE	
DIMENSIONS ARE IN MILLIMETERS	DRAWN	Ryan W.	11/8/2019	TITLE:
TOLERANCES: ±3.0	CHECKED			Shoulder Bevel Gear (1)
	ENG APPR.			
	MFG APPR.			
INTERPRET GEOMETRIC TOLERANCING PER:	Q.A.			
MATERIAL PLA, 20% Infill	COMMENTS:			SIZE A
FINISH N/A				DWG. NO.
				REV 1.0
DO NOT SCALE DRAWING				SCALE: 2:3
				WEIGHT:
				SHEET 5 OF 18

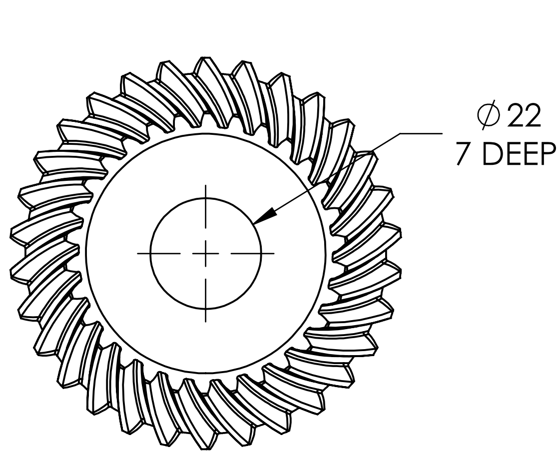

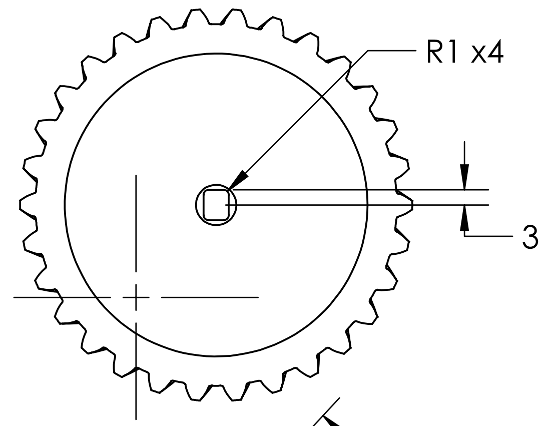

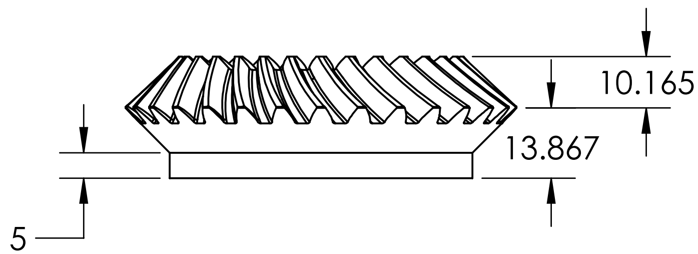

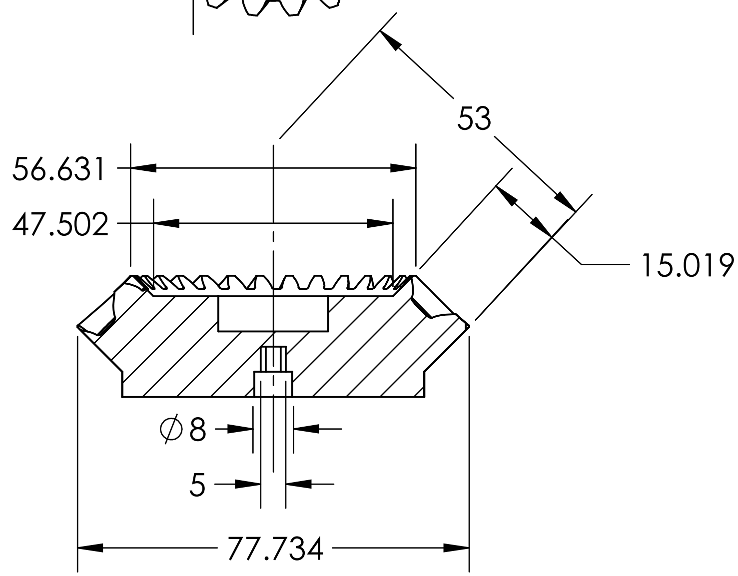

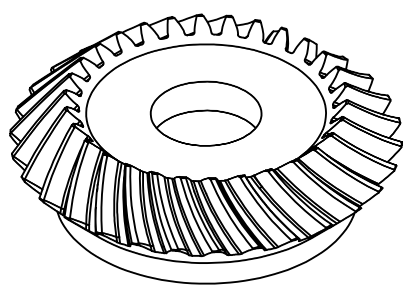

UNLESS OTHERWISE SPECIFIED:		NAME	DATE
DIMENSIONS ARE IN MILLIMETERS TOLERANCES: ±3.0	DRAWN	Ryan W.	11/8/2019
	CHECKED		
	ENG APPR.		
	MFG APPR.		
INTERPRET GEOMETRIC TOLERANCING PER:	Q.A.		
MATERIAL PLA, 20% Infill	COMMENTS:		
FINISH N/A			
DO NOT SCALE DRAWING			

TITLE:

Shoulder Bevel Gear (2)

SIZE	DWG. NO.	REV
A		1.0

SCALE: 2:3	WEIGHT:	SHEET 6 OF 18

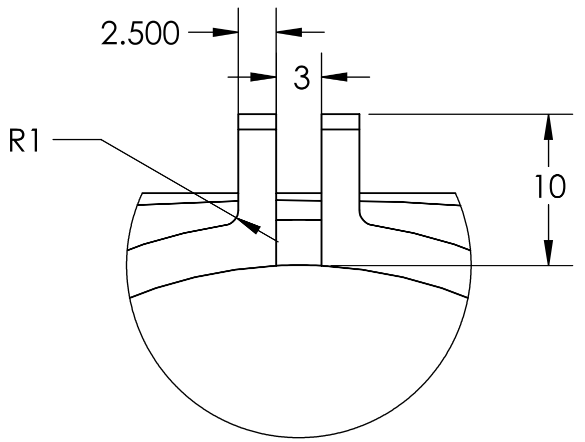

SCALE 2:1

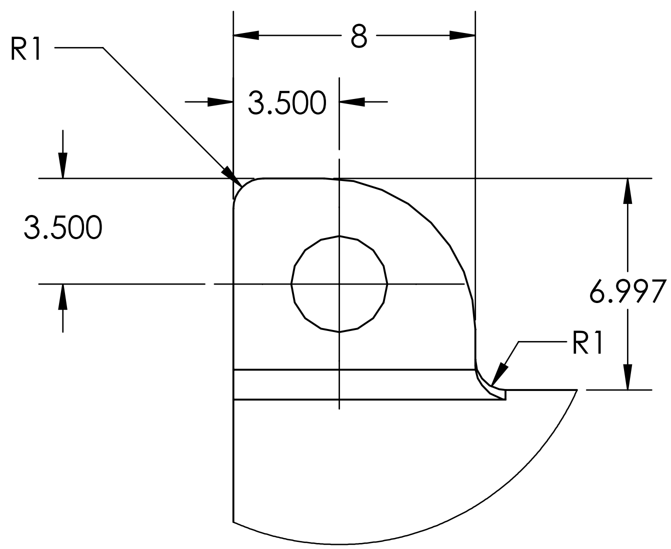

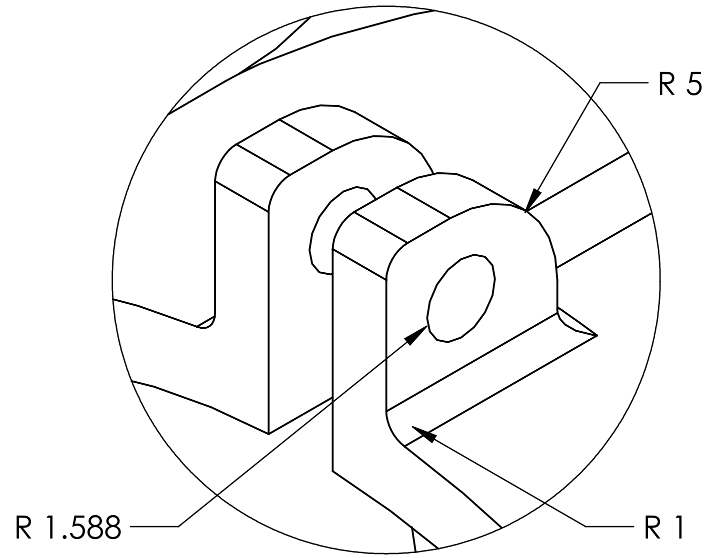

UNLESS OTHERWISE SPECIFIED:		NAME	DATE	
DIMENSIONS ARE IN MILLIMETERS	DRAWN	Ryan W.	11/20/2019	
TOLERANCES: ±3.0	CHECKED			TITLE:
	ENG APPR.			CLAMP DESIGN
	MFG APPR.			
INTERPRET GEOMETRIC TOLERANCING PER:	Q.A.			
MATERIAL PLA	COMMENTS: THIS DRAWING SHOWS THE CLAMPING MECHANISM TO BE USED FOR LINK 2_A, LINK 2_B, LINK 3_A, AND LINK 3_B.			SIZE A; DWG. NO.; REV 1.0
FINISH N/A				
DO NOT SCALE DRAWING				SCALE: 4:1 WEIGHT: SHEET 7 OF 18

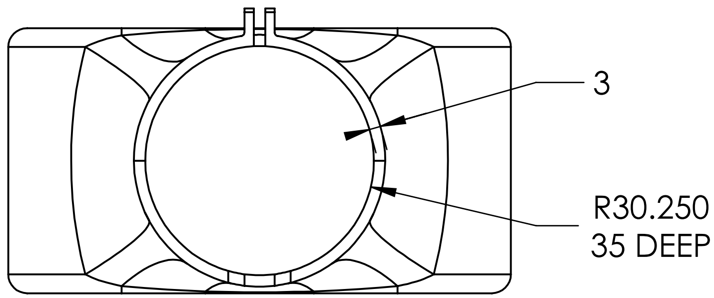

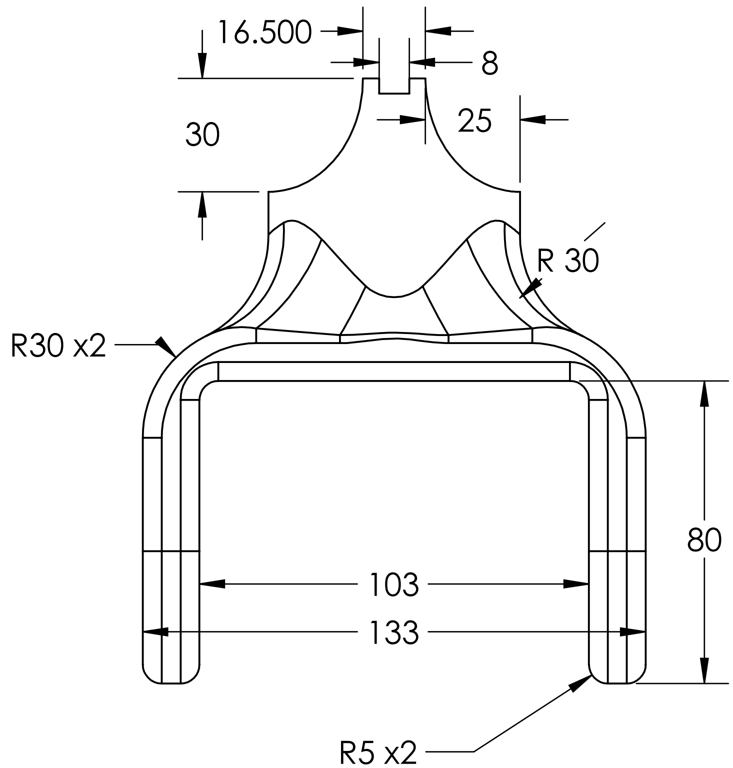

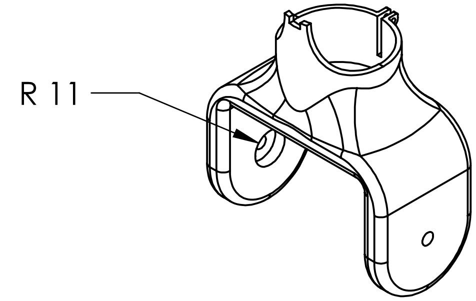

SCALE 1:4

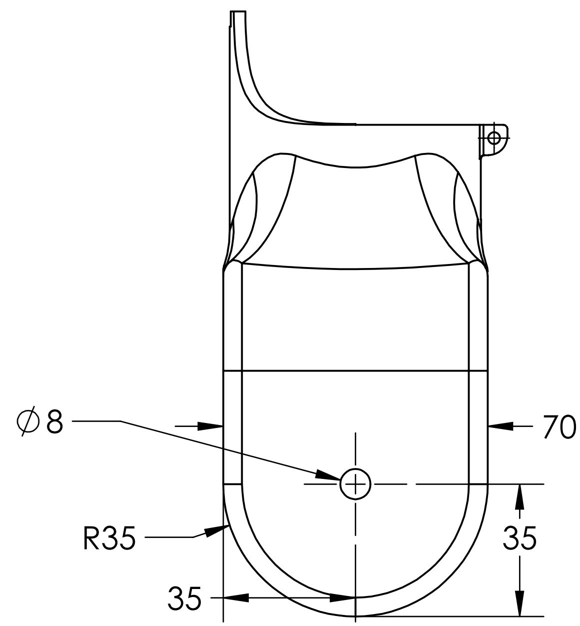

UNLESS OTHERWISE SPECIFIED:		NAME	DATE	
DIMENSIONS ARE IN MILLIMETERS TOLERANCES: ±3.0	DRAWN	Ryan W.	11/11/2019	TITLE: Link 2_a
	CHECKED			
	ENG APPR.			
	MFG APPR.			
	Q.A.			
INTERPRET GEOMETRIC TOLERANCING PER:	COMMENTS:			SIZE A — DWG. NO. — REV 1.0
MATERIAL PLA, 30% Infill				
FINISH N/A				
DO NOT SCALE DRAWING				SCALE: 1:2 — WEIGHT: — SHEET 8 OF 18

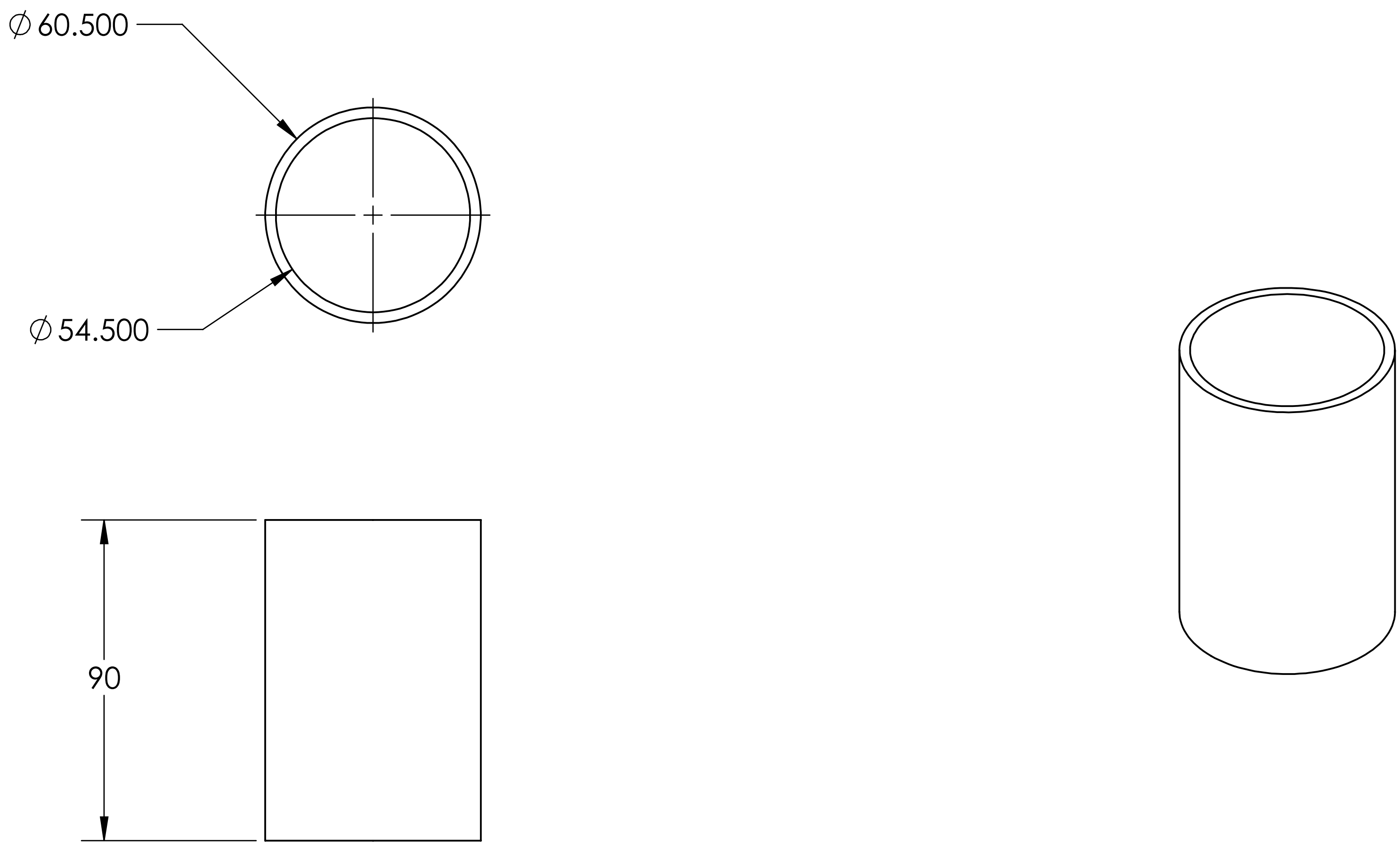

UNLESS OTHERWISE SPECIFIED:			DATE
DIMENSIONS ARE IN MILLIMETERS TOLERANCES: ±3.0	DRAWN	Ryan W.	11/11/2019
	CHECKED		
	ENG APPR.		
	MFG APPR.		
INTERPRET GEOMETRIC TOLERANCING PER:	Q.A.		
MATERIAL Aluminum	COMMENTS:		
FINISH N/A			
DO NOT SCALE DRAWING			

TITLE: Link 2 Tubing

SIZE	DWG. NO.	REV
A		1.0

SCALE: 1:2 WEIGHT: SHEET 9 OF 18

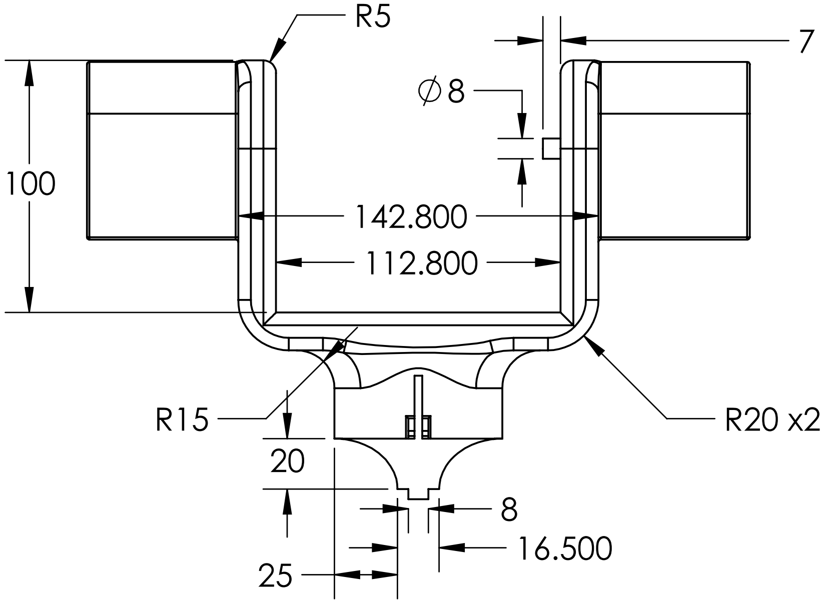

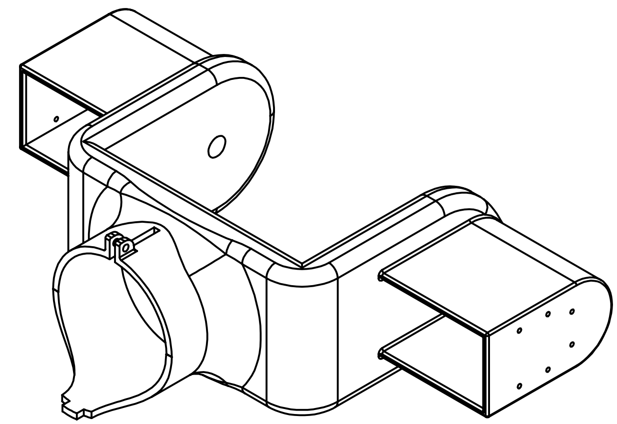

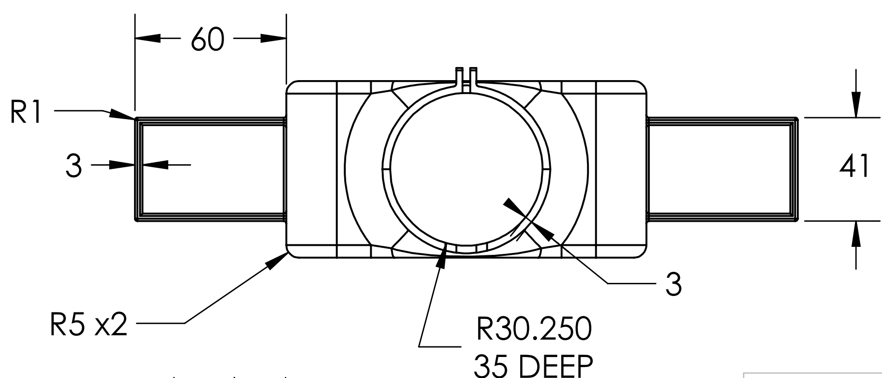

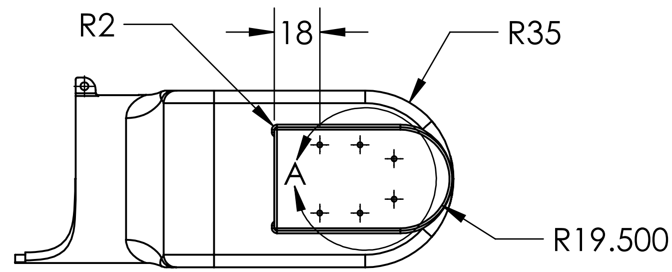

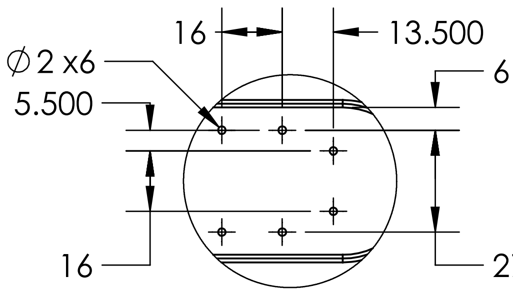

DETAIL A
SCALE 1 : 2

UNLESS OTHERWISE SPECIFIED:		NAME	DATE	
DIMENSIONS ARE IN MILLIMETERS TOLERANCES: ±3.0	DRAWN	Ryan W.	11/13/2019	
	CHECKED			TITLE: Link 2_b
	ENG APPR.			
	MFG APPR.			
INTERPRET GEOMETRIC TOLERANCING PER:	Q.A.			
MATERIAL: PLA, 30% Infill	COMMENTS:			SIZE A | DWG. NO. | REV 1.0
FINISH: N/A				
DO NOT SCALE DRAWING				SCALE: 1:3 | WEIGHT: | SHEET 10 OF 18

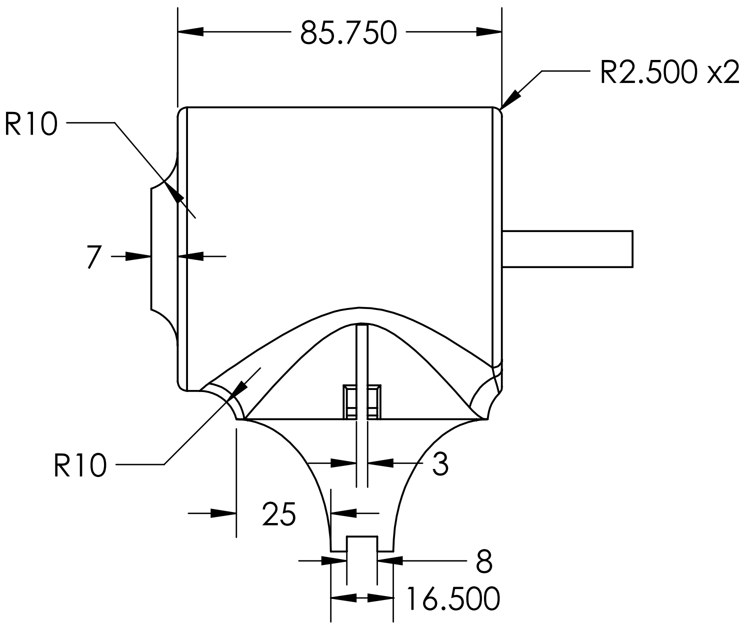

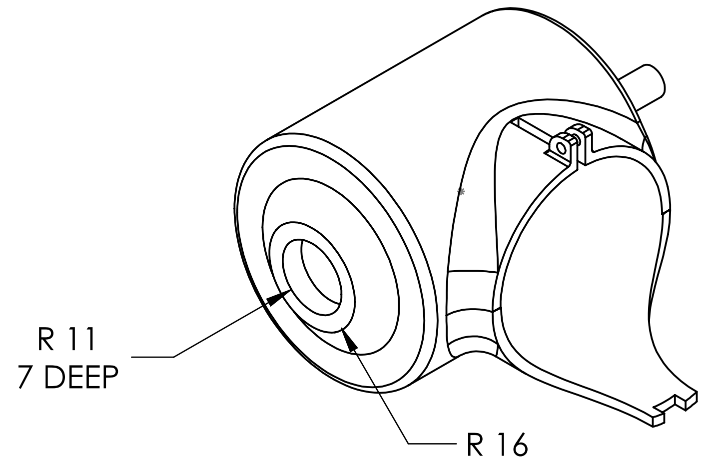

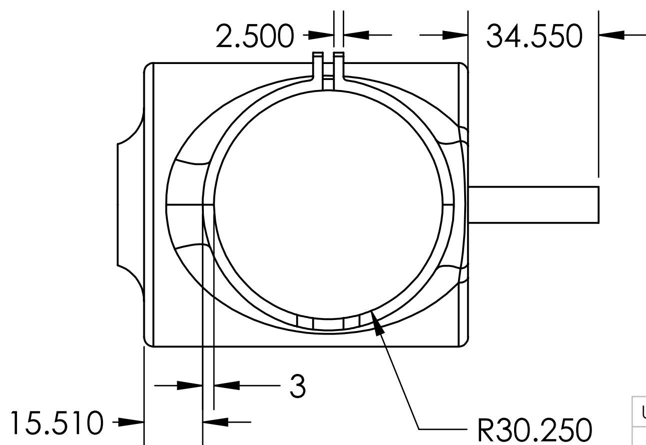

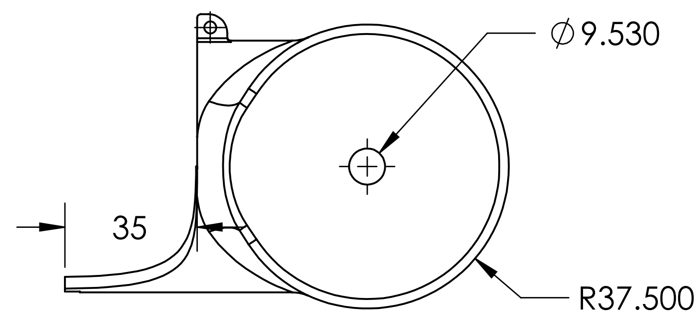

UNLESS OTHERWISE SPECIFIED:		NAME	DATE	
DIMENSIONS ARE IN MILLIMETERS TOLERANCES: ±3.0	DRAWN	Ryan W.	11/11/2019	
	CHECKED			TITLE:
	ENG APPR.			Link 3_a
	MFG APPR.			
INTERPRET GEOMETRIC TOLERANCING PER:	Q.A.			
MATERIAL PLA, 30% Infill	COMMENTS:			SIZE A · DWG. NO. · REV 1.0
FINISH N/A				
DO NOT SCALE DRAWING				SCALE: 1:2 · WEIGHT: · SHEET 11 OF 18

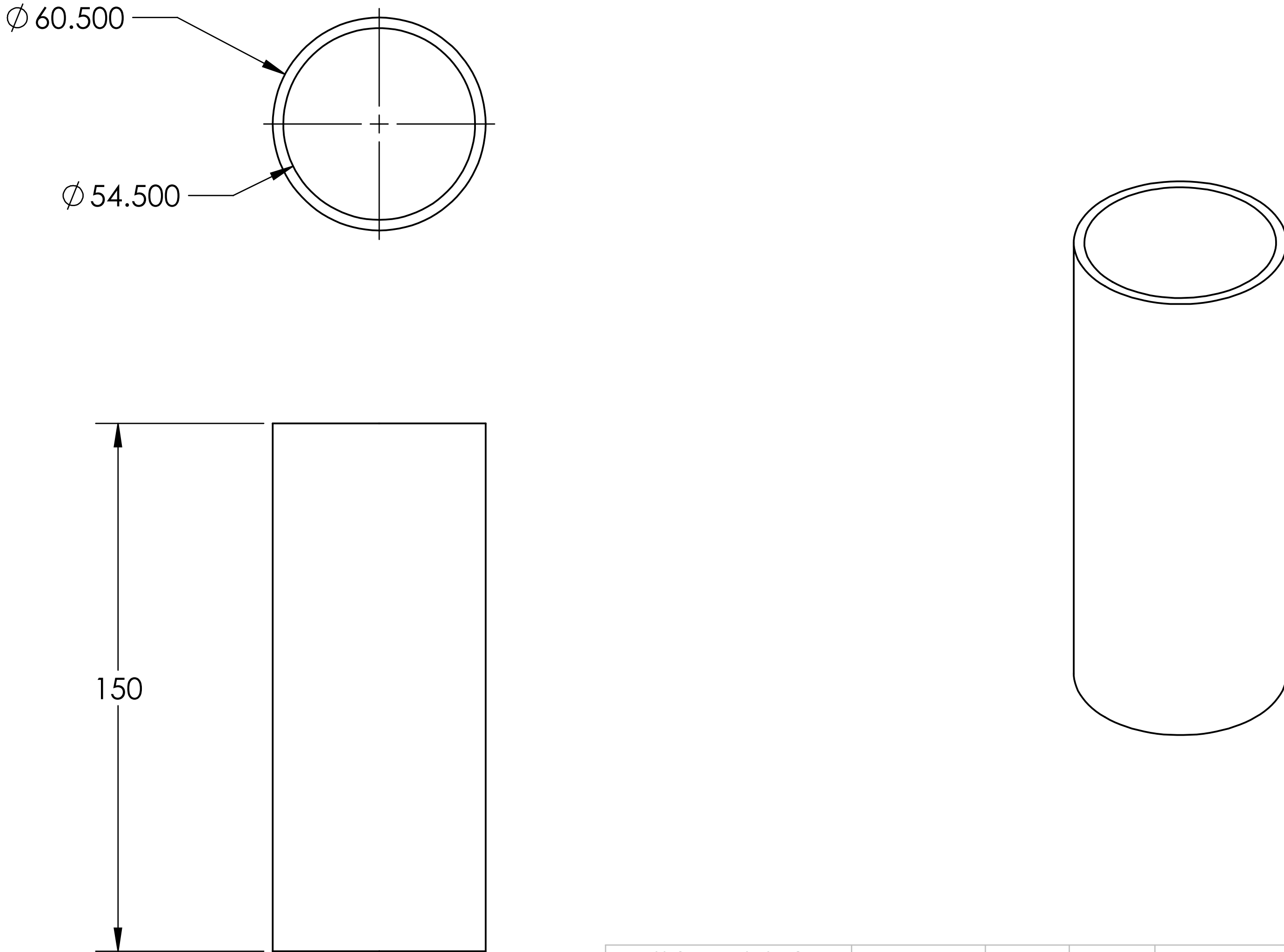

UNLESS OTHERWISE SPECIFIED:		NAME	DATE	
DIMENSIONS ARE IN MILLIMETERS TOLERANCES: ±3.0	DRAWN	Ryan W.	11/11/2019	
	CHECKED			TITLE: Link 3 Tubing
	ENG APPR.			
	MFG APPR.			
INTERPRET GEOMETRIC TOLERANCING PER:	Q.A.			
MATERIAL Aluminum	COMMENTS:			SIZE A — DWG. NO. — REV 1.0
FINISH N/A				
DO NOT SCALE DRAWING				SCALE: 1:5 — WEIGHT: — SHEET 12 OF 18

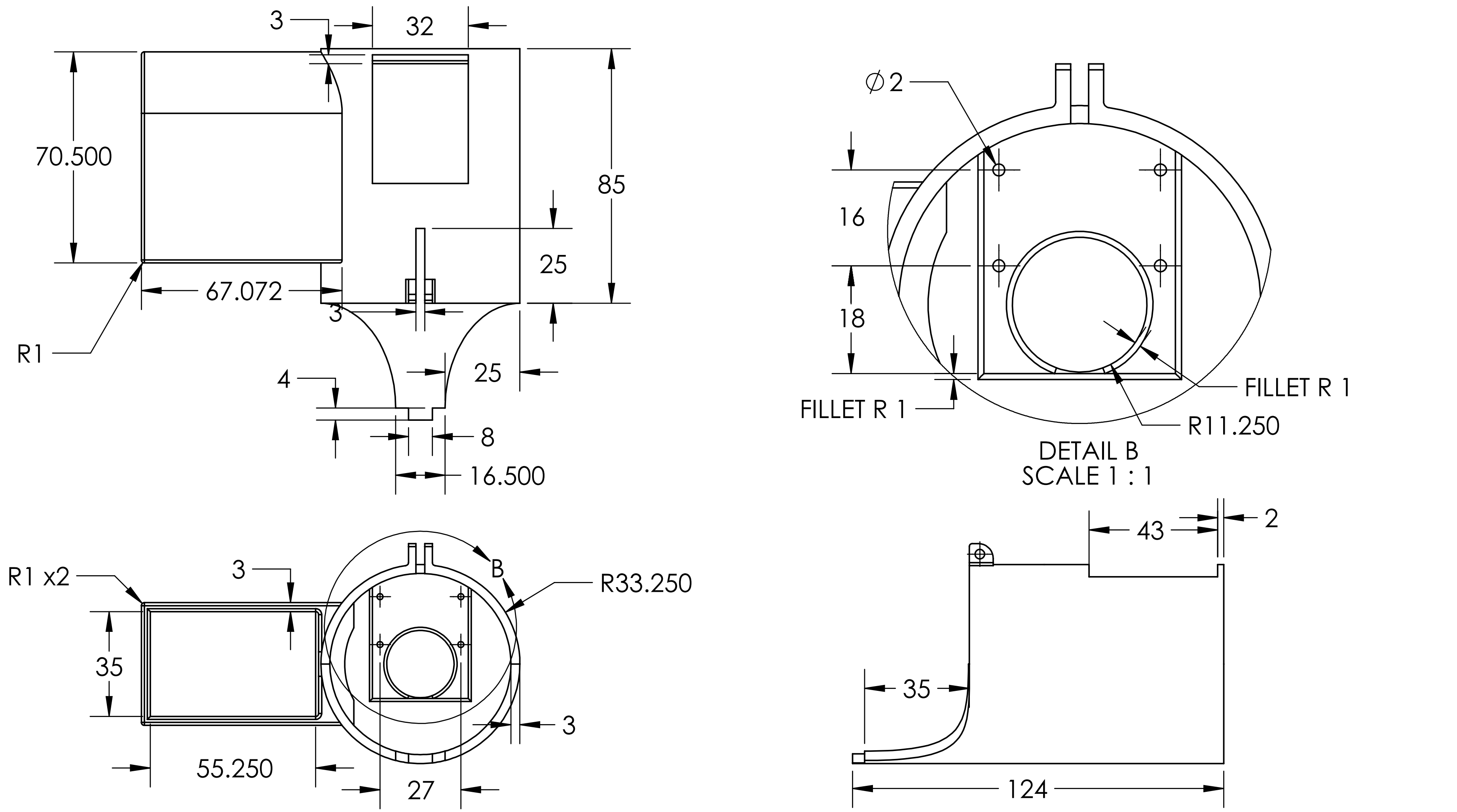

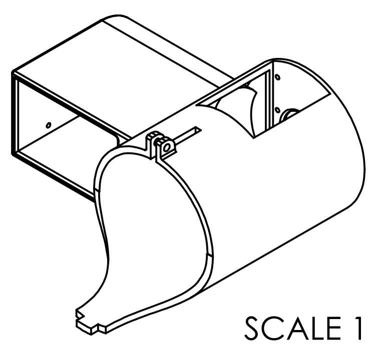

SCALE 1:3

UNLESS OTHERWISE SPECIFIED:		NAME	DATE	
DIMENSIONS ARE IN MILLIMETERS TOLERANCES: ±3.0	DRAWN	Ryan W.	11/15/2019	TITLE: Link 3_b
	CHECKED			
	ENG APPR.			
	MFG APPR.			
	Q.A.			
INTERPRET GEOMETRIC TOLERANCING PER:	COMMENTS:			
MATERIAL PLA, 30% Infill				SIZE A — DWG. NO. — REV 1.0
FINISH N/A				
DO NOT SCALE DRAWING				SCALE: 1:2 — WEIGHT: — SHEET 13 OF 18

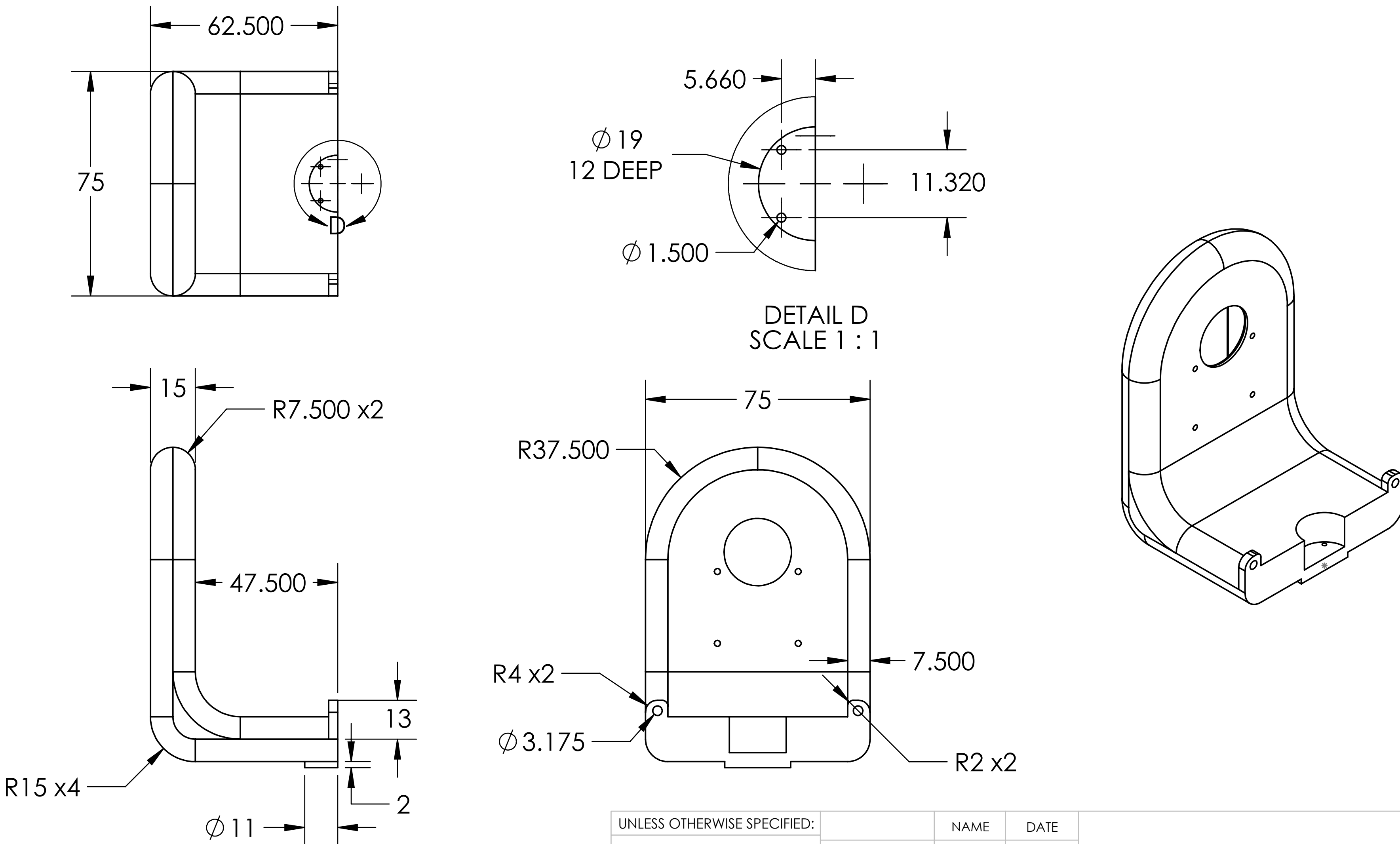

UNLESS OTHERWISE SPECIFIED:		NAME	DATE	
DIMENSIONS ARE IN MILLIMETERS	DRAWN	Ryan W.	11/11/2019	
TOLERANCES: ±3.0	CHECKED			TITLE: Link 4
	ENG APPR.			
	MFG APPR.			
INTERPRET GEOMETRIC TOLERANCING PER:	Q.A.			
MATERIAL PLA, 30% Infill	COMMENTS:			SIZE A — DWG. NO. — REV 1.0
FINISH N/A				
DO NOT SCALE DRAWING				SCALE: 1:2 — WEIGHT: — SHEET 14 OF 18

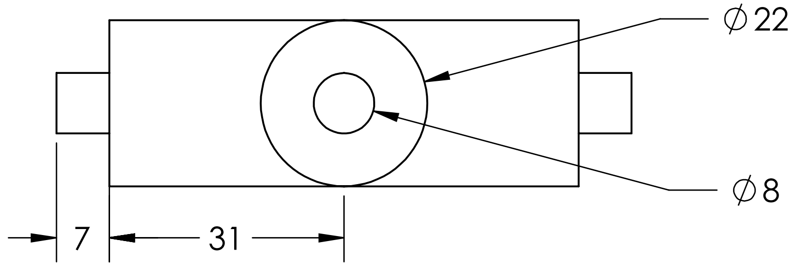

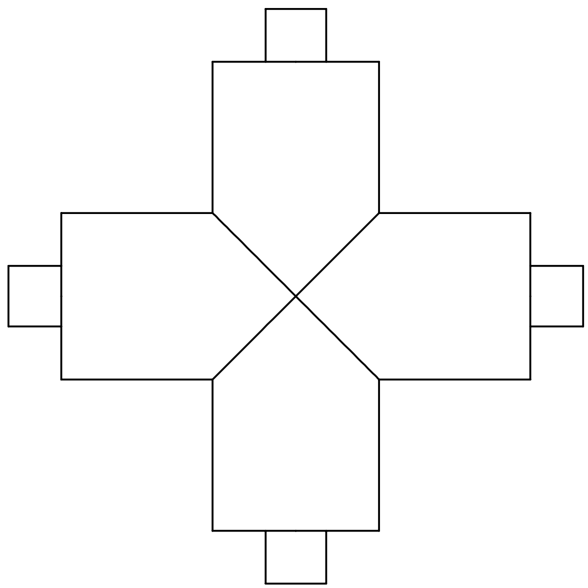

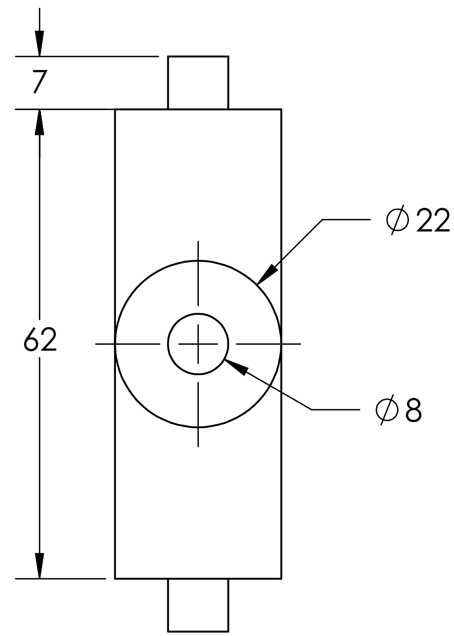

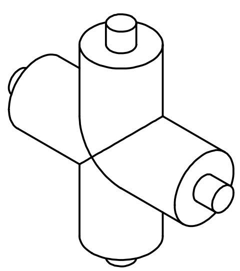

SCALE 1:2

UNLESS OTHERWISE SPECIFIED:		NAME	DATE	
DIMENSIONS ARE IN MILLIMETERS TOLERANCES: ±3.0	DRAWN	Ryan W.	11/8/2019	TITLE: Wrist Differential Crossbar
	CHECKED			
	ENG APPR.			
	MFG APPR.			
	Q.A.			
INTERPRET GEOMETRIC TOLERANCING PER:	COMMENTS:			SIZE A
MATERIAL PLA, 30% Infill				DWG. NO.
FINISH N/A				REV 1.0
DO NOT SCALE DRAWING				SCALE: 1:1 · WEIGHT: · SHEET 15 OF 18

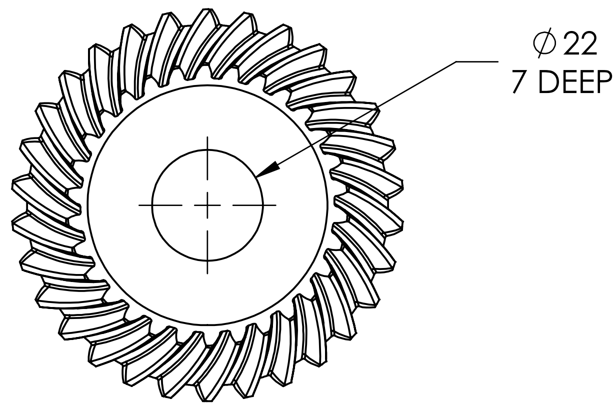

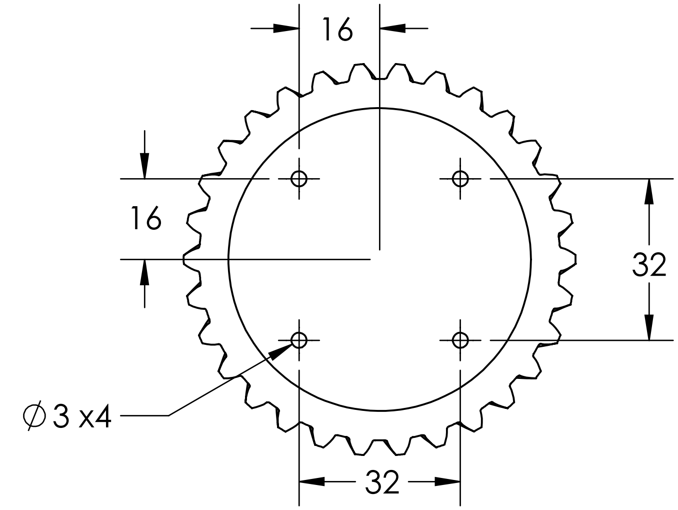

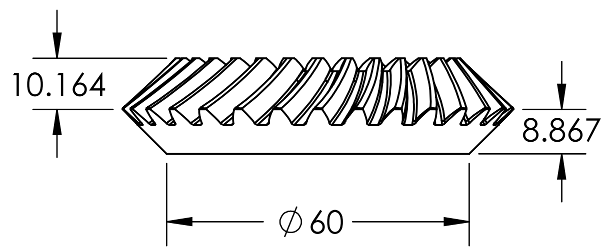

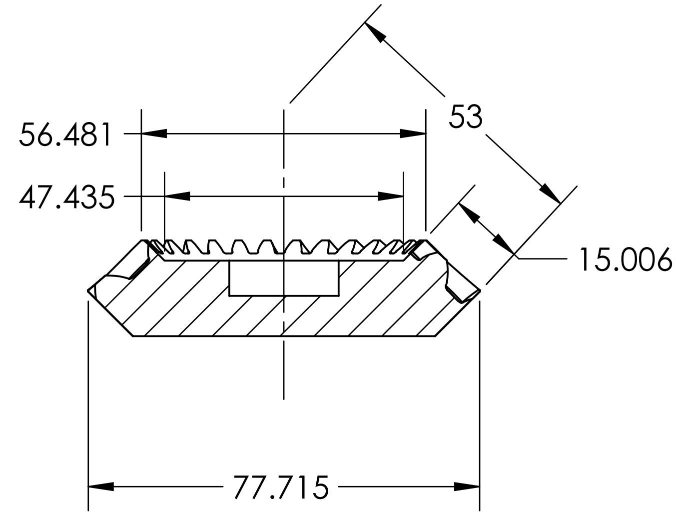

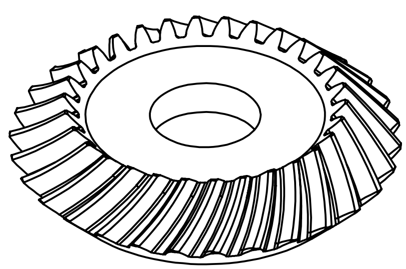

UNLESS OTHERWISE SPECIFIED:		NAME	DATE	
DIMENSIONS ARE IN MILLIMETERS	DRAWN	Ryan W.	11/8/2019	TITLE:
TOLERANCES: ±3.0	CHECKED			Wrist Bevel Gear (1)
	ENG APPR.			
	MFG APPR.			
INTERPRET GEOMETRIC TOLERANCING PER:	Q.A.			
MATERIAL PLA, 20% Infill	COMMENTS:			SIZE A / DWG. NO. / REV 1.0
FINISH N/A				
DO NOT SCALE DRAWING				SCALE: 2:3 / WEIGHT: / SHEET 16 OF 18

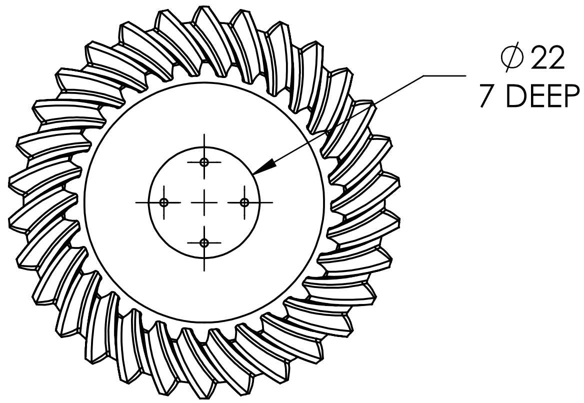

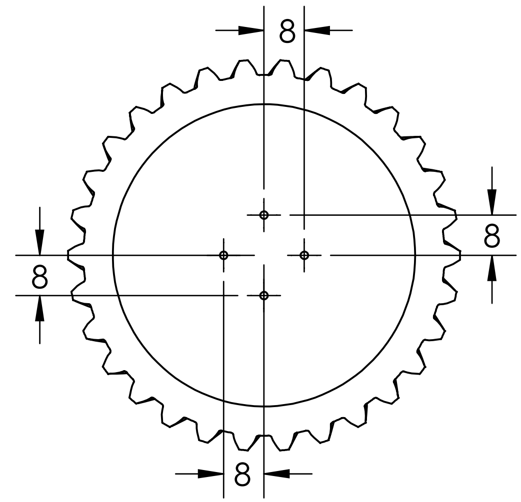

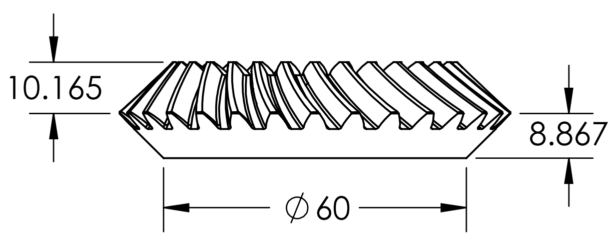

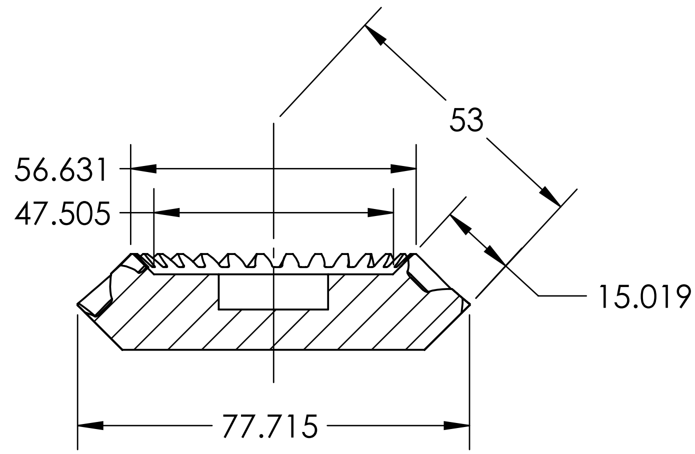

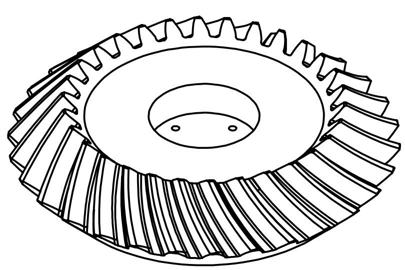

UNLESS OTHERWISE SPECIFIED:		NAME	DATE	
DIMENSIONS ARE IN MILLIMETERS	DRAWN	Ryan W.	11/8/2019	TITLE:
TOLERANCES: ±3.0	CHECKED			Wrist Bevel Gear (2)
	ENG APPR.			
	MFG APPR.			
INTERPRET GEOMETRIC TOLERANCING PER:	Q.A.			
MATERIAL PLA, 20% Infill	COMMENTS:			SIZE A · DWG. NO. · REV 1.0
FINISH N/A				
DO NOT SCALE DRAWING				SCALE: 2:3 · WEIGHT: · SHEET 17 OF 18

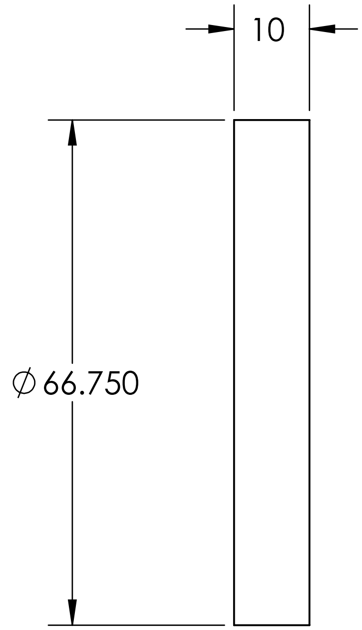

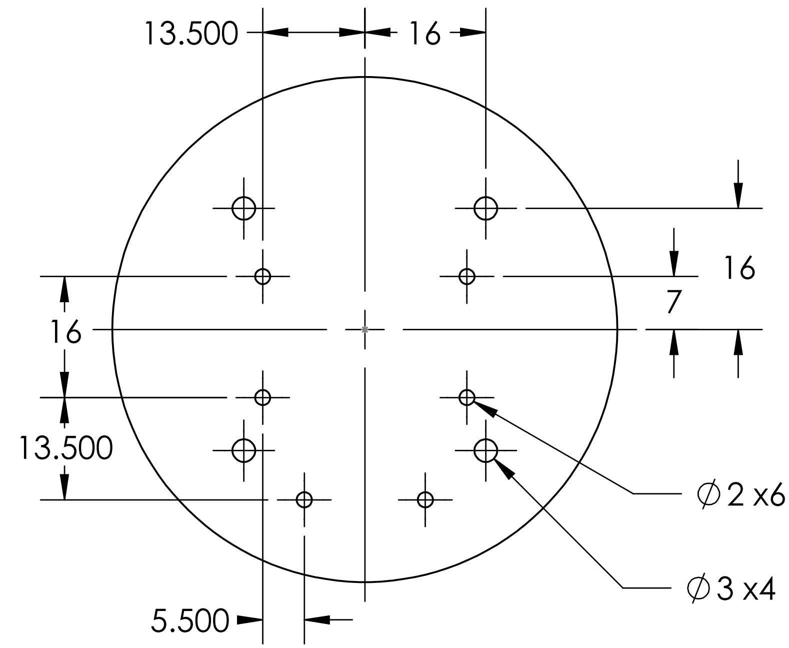

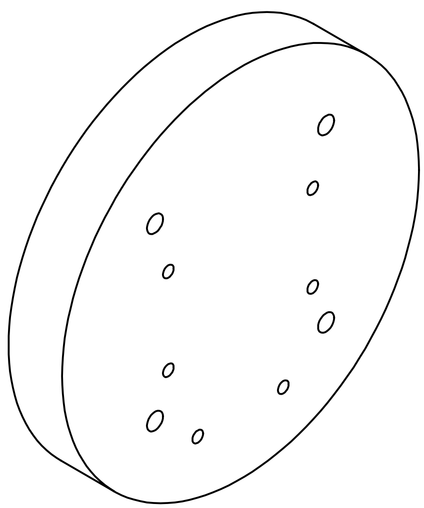

UNLESS OTHERWISE SPECIFIED:

DIMENSIONS ARE IN MILLIMETERS

TOLERANCES: ±3.0

INTERPRET GEOMETRIC TOLERANCING PER:

MATERIAL: PLA, 20% Infill

FINISH: N/A

DO NOT SCALE DRAWING

	NAME	DATE
DRAWN	Ryan W.	11/11/2019
CHECKED		
ENG APPR.		
MFG APPR.		
Q.A.		

COMMENTS:

TITLE: End Effector

SIZE: A
DWG. NO.
REV: 1.0

SCALE: 1:2
WEIGHT:
SHEET 18 OF 18

A.III Salient Code

Listing 1: Actuator Dynamics MATLAB Code

```matlab
% dynamixel motor model experiment
close all;clear;clc

% test loads mass moments of inertia
m = [.146 .088 0.108];          % mass (kg)
b = [.61277 .37227 0.28257];    % length (m)
h = [.01915 0.01915 0.0299];    % height (m)
J = (1/12)*m.*(h.^2 + b.^2);

% path to csv files relative to script
datapath = 'data/AX12A/';
files = dir(strcat(datapath,'*.csv'));
numFiles = length(files);
% initialize variables
[damp, wn, Tp] = deal(zeros(numFiles,1));

for ii = 1:numFiles
    % load experimental data, skip 5 header lines
        M = csvread(strcat(datapath, files(ii).name),5,0);
    % clean data by removing outliers
        nani = (find(diff(M(:,1)) > 100));
        M(nani,:) = [];
    % show response
         figure();
         plot(M(:,1),M(:,2))
         title('Experimental Data')
    % find % OS
        peak = max(M(:,2));                             % peak value
        peaki = find(M(:,2)==peak, 1, 'first');         % peak value index
        ss = M(end,2);                                  % steady state
        os = ((peak - ss) / ss) * 100;                  % % OS
    % damping ratio
        damp(ii) = -log(os/100) / sqrt(pi^2 + log(os/100)^2);
    % find where the motor begins responding
        start = M(find(diff(M(:,2)) > 1, 1, 'first'), 1);
    % time to peak
        Tp(ii) = (M(peaki,1) - start) / 1000;
    % natural frequency
        wn(ii) = pi / (sqrt(1 - damp(ii)^2)*Tp(ii));
end

sol = zeros(4,1);
```

```
% no load case, 2*zeta*omega_n
sol(1) = 2*mean(damp(end-2:end))*mean(wn(end-2:end));
% no load case, omega_n^2
sol(2) = mean(wn(end-2:end))^2;

% obtain average damping ratio and natural frequencies for load cases
zeta = [mean(damp(1:3));mean(damp(4:6));mean(damp(7:9))];
omegan = [mean(wn(1:3));mean(wn(4:6));mean(wn(7:9))];

alpha = 2.*zeta.*omegan;
beta = omegan.^2;
A = zeros(3,2);
b = zeros(3,1);

for jj = 1:3
    A(jj,:) = [1, -(alpha(jj)*J(jj) + beta(jj)*J(jj))];
    b(jj) = alpha(jj) + beta(jj);
end

sol(3:4) = A \ b;
```

Listing 2: Forward Kinematics MATLAB Function

```
function [r6,T6]= MeiosisFK(theta)

    %       Mapping between joint space and motor space
    N = 10;         %Gear Ratio
    A = [ 1/(2*N), 1/(2*N),   0, 0,   0,   0;
          1/(2*N),-1/(2*N),   0, 0,   0,   0;
                0,       0,-1/N, 0,   0,   0;
                0,       0,   0, 1,   0,   0;
                0,       0,   0, 0,-1/2, 1/2;
                0,       0,   0, 0, 1/2, 1/2];
    gamma = A*theta;

%     %Define Constants
%     LB = 12.275;
%     L1 = 0;
%     L2 = 25;
%     L3 = 20;
%     L4 = 7.2;
%     L5 = 0;
```

```
%     L6 = 5.3;

    %Relative Positions
    rBfromI = [ 0.00000000; 0.00000000; 0.00000000];
    r1fromB = [ 0.00000000; 0.00000000; 0.12275000];
    r2from1 = [ 0.00000000; 0.00000000; 0.00000000];
    r3from2 = [ 0.00000000; 0.25000000; 0.00000000];
    r4from3 = [ 0.00000000; 0.20000000; 0.00000000];
    r5from4 = [ 0.00000000; 0.07000000; 0.00000000];
    r6from5 = [ 0.00000000; 0.04750000; 0.00000000];
    %r7from6 = [0;       0;       0]; % dist. from 3rd wrist coor. frame to
       the end effector is 5.25 cm

    %Orientations wrt I:
    T1 = rotz(gamma(1));
    T2 = T1*rotx(gamma(2));
    T3 = T2*rotx(gamma(3));
    T4 = T3*roty(gamma(4));
    T5 = T4*rotx(gamma(5));
    T6 = T5*roty(gamma(6));

    %Positions wrt I:
    %rB = rBfromI;
    r1 = r1fromB;
    r2 = r1 + T1*r2from1;
    r3 = r2 + T2*r3from2;
    r4 = r3 + T3*r4from3;
    r5 = r4 + T4*r5from4;
    r6 = r5 + T5*r6from5;

end
```

Listing 3: Inverse Kinematics MATLAB Function

```
function [theta, error] = MeiosisIK(pos,R)

    eOff = [0;47.5;0];
    npos = pos - R*eOff;
    xc = npos(1);
    yc = npos(2);
    zc = npos(3);
    L1 = 122.75;
```

```
    d = 0;
    L2 = 250;
    L3 = 270;

    % Inverse Position
    if (xc^2 + yc^2 -d^2) < 0
        theta = 1000*[1;1;1;1;1;1];
        error = 1;
    else
        t1 = atan2(yc,xc) - atan2(d,sqrt(xc^2 + yc^2 -d^2)) - pi/2;
        D = (xc^2 + yc^2 - d^2 + (zc - L1)^2 - L2^2 - L3^2)/(2*L2*L3);
        t3 = atan2(-sqrt(1-D^2),D);
        t2 = atan2(zc - L1,sqrt(xc^2 + yc^2 - d^2)) - atan2(L3*sin(t3),L2 + L3*cos(t3));

        % Inverse Orientation
        T3 = rotz(t1)*rotx(t2)*rotx(t3);
        T = T3.'*R;
        t6 = atan2(T(2,1),-T(2,3));
        t4 = atan2(T(1,2),T(3,2));
        %t4 = atan2(sin(t4),cos(t4));

        if sin(t4) > -10e-6 && sin(t4) < 10e-6
            t5 = atan2(T(3,2)/cos(t4),T(2,2));
        else
            t5 = atan2(T(1,2)/sin(t4),T(2,2));
        end

        gamma = [t1,t2,t3,t4,t5,t6].';

        %       Mapping between joint space and motor space
        N = 10;         %Gear Ratio
%         B = [ N, N, 0, 0, 0, 0;
%               N,-N, 0, 0, 0, 0;
%               0, 0,-N, 0, 0, 0;
%               0, 0, 0, 1, 0, 0;
%               0, 0, 0, 0,-1, 1;
%               0, 0, 0, 0, 1, 1];
        A = [ 1/(2*N), 1/(2*N),   0, 0,   0,   0;
          1/(2*N),-1/(2*N),   0, 0,   0,   0;
                0,       0,-1/N, 0,   0,   0;
                0,       0,   0, 1,   0,   0;
                0,       0,   0, 0,-1/2, 1/2;
                0,       0,   0, 0, 1/2, 1/2];

```

```
        theta = A\gamma;
        error = 0;
    end
end
```